ABSTRACT

Title of Dissertation: DEVELOPING HIGHLY ACCURATE AND STABLE OPEN-REGION ELECTROMAGNETIC SIMULATIONS

Xin Wu, Doctor of Philosophy, 2003

Dissertation directed by: Assistant Professor Omar M. Ramahi
Department of Mechanical Engineering, and Department of Electrical and Computer Engineering

In open-region electromagnetic simulations, the computational domain has to be truncated by an absorbing boundary condition (ABC) to model the infinite space. The performance of ABC strongly affects the accuracy of overall numerical simulation. For a class of advanced problems demanding high accuracy, such as in the modeling of medical detection devices, indoor wireless communication systems and remote sensing equipments, the received signal can be several orders of magnitude less than the transmitted signal. Furthermore, wide-band simulations require long running times for transients-based simulations, which increase the potential for instability. Therefore, accuracy and stability of absorbing boundary conditions are identified as critical in the design of numerical algorithms compatible with advanced applications.

In this work, theory of Concurrent Complementary Operators Method (C-COM) in both transient and frequency-domain numerical simulations is investigated. The C-COM is based on the basic premise of primary reflection cancellation. The C-COM applications to numerically derived ABCs in finite difference time-domain (FDTD)

method, and to frequency domain ABCs in both finite difference frequency domain (FDFD) method and finite element method (FEM) method are developed. Extensive numerical experiments are conducted showing dramatic increase in accuracy when the C-COM is applied in comparison to previous published techniques.

Previous works that addressed the boundary instability arising from the application of the absorbing boundary condition used either the von Neumann analysis or the Gustafsson-Kreiss-Sundström (GKS) analysis. These earlier works, however, did not explain the inconsistencies that have been observed between the theoretical predictions and numerical experiments. This thesis presents a new stability analysis applicable to boundary conditions. This new analysis, referred to as Coupled Stability Analysis (CSA), is based on the fundamental assumption that absorbing boundary conditions are not perfect, and therefore, generate waves that reflect back into the computational domain. It is found that this analysis yields results that are fully consistent with those obtained from numerical experiments. As an important consequence of this analysis, and contrary to earlier conjectures, we show that Higdon's absorbing boundary condition of order 3 (and possibly, higher orders) to be unconditionally unstable.

DEVELOPING HIGHLY ACCURATE AND STABLE OPEN-REGION ELECTROMAGNETIC SIMULATIONS

By

Xin Wu

Dissertation submitted to the Faculty of the Graduate School of the
University of Maryland at College Park in partial fulfillment
of the requirements for the degree of
Doctor of Philosophy
2003

Advisory Committee:

Professor Omar M. Ramahi, Chair/Advisor
Professor Thomas M. Antonsen
Professor Neil Goldsman
Professor Peter Sandborn
Professor Elias Balaras
Dr. Parvez N. Guzdar

ACKNOWLEDGEMENTS

My Ph.D dissertation is a result of three years of hard work through which I have been accompanied and supported by many people. It is my pleasure to have the opportunity to express my gratitude to all of them.

First, I would like to thank my advisor, Dr. Omar M. Ramahi, for his guidance and support throughout my doctoral study, for his wisdom, open mind, and illuminations when I need most, for his encouragement, and help to complete my research work successfully.

Second, I would like to thank Dr. Thomas M. Antonsen, Dr. Neil Goldsman, Dr. Peter Sandborn, Dr. Elias Balaras, and Dr. Parvez N. Guzdar for kindly consenting to be on my thesis committee and their time, suggestions and comments. Also, I would like to thank Dr. Quirino Balzano for giving suggestions on my research work.

In addition, I would like to express thanks to all my colleagues in the Electromagnetic Compatibility and Propagation Lab, CALCE Electronic Products and Systems Center, and Department of Mechanical Engineering, for their valuable help and friendship.

Last but certainly not least, I am especially indebted to my wife, my parents, my sister for their encouragement, support, and love, as always.

TABLE OF CONTENTS

LIST OF FIGURES

I. INTRODUCTION

I.1 OPEN-REGION ELECTROMAGNETIC SIMULATIONS

Second-order linear partial differential equations (PDEs) can be classified as elliptic, hyperbolic, or parabolic, depending on the coefficients of the equation. Examples of the physical phenomena described by the second-order PDEs include fluid dynamics, electromagnetics, acoustics, diffusion and heat flow, neutron diffusion and radiation transfer, and elastic wave in solids, … etc. [1]-[3]. Only very narrow range of real world physical problems can be solved using analytical methods such as separation of variables, integral solutions and series of expansion. Numerical methods are important tools to deal with the majority of real-world problems, which are not solvable analytically. For the hyperbolic and parabolic problems, one of the popular numerical techniques is based on finite difference approximation of the partial derivatives, which gives an approximation of the PDEs directly. With the introduction of variational methods, PDEs can also be constructed as equivalent functionals. The variational methods form a common base for the Finite Element Method (FEM) and Weighted Residual Method (WRM). If integral forms of PDEs can be constructed, Boundary Element Method (BEM), or WRM can be used. The commonly used numerical methods for the physical phenomena described by the 2^{nd} order PDEs are illustrated in Fig. 1.

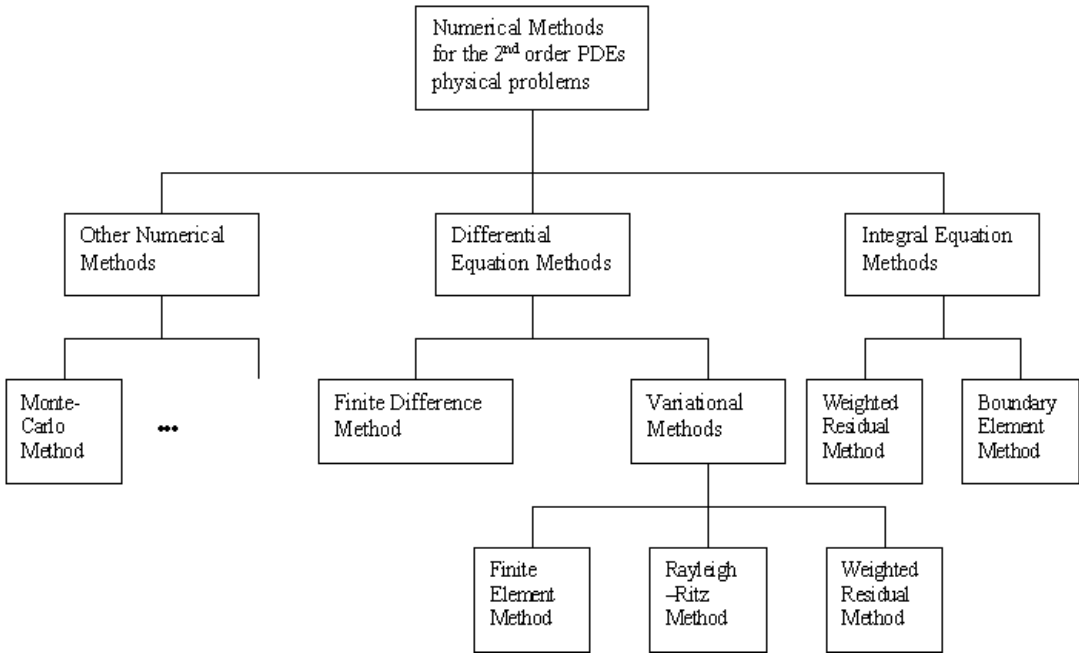

Fig. 1. Numerical methods used to solve physical problems described by the 2nd order PDEs.

The hyperbolic or parabolic problems are usually spatially large or infinite space problems. Using numerical simulations to model these problems over infinite domain is impossible due to limited computational resources. Therefore, the computational domain has to be truncated to a finite size and on the truncated boundary, artificial boundary conditions needs to be applied to model the infinite space. For practical problems, the computational domain needs to be truncated as close as possible to the radiating objects to save time and computational resources. Fig. 2 shows how an artificial boundary condition is applied to the truncated boundary to simulate the infinite space. The artificial boundary conditions applied to the truncated computational domain are named absorbing boundary conditions (ABCs), non-reflecting boundary conditions (NRBCs), or radiation boundary conditions (RBCs).

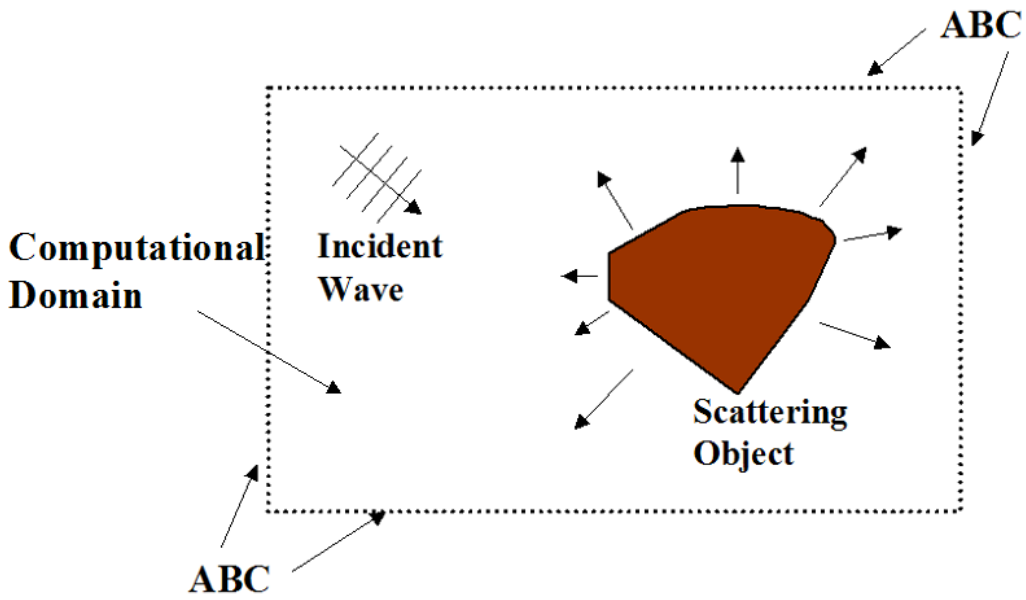

Fig. 2. Illustration of an open-region simulation.

The solution to electromagnetic (EM) wave propagation is governed by Maxwell's equations given by

$$\begin{aligned} \nabla \times \mathbf{E} &= -\mu \frac{\partial \mathbf{H}}{\partial t} \\ \nabla \times \mathbf{H} &= \varepsilon \frac{\partial \mathbf{E}}{\partial t} + \mathbf{J} \\ \nabla \bullet \mathbf{D} &= \rho \\ \nabla \bullet \mathbf{B} &= \mathbf{0} \end{aligned} \qquad (1)$$

where **E** is the electric field, **H** is the magnetic field, t is time, μ and ε are the permeability and permittivity of medium, respectively, **J** is the volume current density, **D** is the electric flux density, **B** is the magnetic flux density, and ρ is the volume charge density. Maxwell's equations are coupled first-order differential equations representing a hyperbolic system [4][5].

I.2 MESH TRUNCATION TECHNIQUES IN OPEN-REGION ELECTROMAGNETIC SIMULATIONS

In computational electromagnetics, the Finite Difference Time-Domain (FDTD) method, the Finite-Difference Frequency Domain (FDFD) method, and the Finite Element Method (FEM) are widely used finite volume numerical techniques. When applying these numerical methods to an open-region EM simulation, artificial boundary conditions are necessary to terminate the truncated computational domain.

Based on the method by which these artificial boundary conditions are constructed, they can be classified as analytically derived absorbing boundary conditions, numerically derived absorbing boundary conditions, or absorbing media. Boundary conditions strongly affect the accuracy of the overall simulation as has been documented extensively in numerous publications [1]-[15].

The major challenge in the construction of ABCs includes two aspects: accuracy and stability. The higher accuracy an ABC can achieve, the less the reflected error will influence the simulation results. As any ABC generates reflections, the reflected fields, when interfering with the interior physical fields, results in instability. Intensive research showed that the current boundary conditions are still not accurate enough to achieve sufficient levels of accuracy. For instance, in high resolution sensing applications, medical non-destructive detection, and indoor wireless communication systems, the detected/received signals can be several orders of magnitude less than the transmitted signals. Therefore, in the numerical simulation of such systems, ABCs generating a

reflection as low as 1/100 (or −40 dB) with respect to the transmitted signals might not be sufficient to achieve the accuracy requirements of the system.

A solution for problems where high accuracy is required is the Concurrent Complementary Operators Method (C-COM). Originally proposed in 1995, the Complementary Operators Method (COM) is simple, flexible, and efficient [16]. The COM operators were also extended to the general analytical ABCs in FDTD. The complementary operation can annihilate the first order reflections from an existing ABC. Compare with other artificial boundary conditions, the COM is the only technique which can effectively minimize the effects of evanescent wave. When compared with other ABCs, it needs approximately twice as much the CPU time, computer memory, or storage space.

To take advantage of the strong absorption properties of the COM method and to avoid the extra consumption of computer resources, the concurrent complementary operators method (C-COM) was developed. The C-COM method averages the two independent complementary operations on an interface inside the computational domain. The C-COM method had already been successfully demonstrated on analytically derived ABCs such as Higdon's ABC in time domain methods [17], and frequency domain finite difference method [18]. The C-COM has been used for guided microwave structure and optical beam modeling in which high accuracy is required [19].

I.3 ABSORBING BOUNDARY CONDITIONS

The complementary operators method and its concurrent version are developed based on the average of two complementary operations developed for an existing

absorbing boundary condition (ABC). From the previous section, the ABCs can be derived either analytically or numerically.

I.3.1 Analytically Derived Absorbing Boundary Conditions

The analytically derived ABC is based on the one-way wave equation. A one-way wave equation describes the behavior of a wave propagating in only one direction. A one-way wave equation describes a wave propagating along the *x*-direction in free space is given as

$$(\partial_x + \frac{1}{c}\partial_t)U = 0 \tag{2}$$

where ∂_x is the partial derivative in *x*, ∂_t is the partial derivative in time *t*, *c* is the light speed, and *U* is the unknown field. The one-way wave equation represents a first order, perfect absorbing boundary condition for a plane wave propagating along the *x*-direction. This can be demonstrated as following:

A plane wave propagating along the *x*-direction can be written as

$$U = e^{j\omega t - jk_x x - jk_y y} + R\ e^{j\omega t + jk_x x - jk_y y} \tag{3}$$

where, ω is the radian frequency, *R* is the reflection coefficient that is generated by the imperfection of a boundary condition and it expresses the amplitude of the reflected wave relative to the amplitude of the incident wave, and k_x is the wave numbers in *x*-directions. Substituting (3) into the one-way wave equation,

$$R = -\frac{-jk_x + j\frac{\omega}{c}}{jk_x + j\frac{\omega}{c}} \tag{4}$$

As the wave is propagating along the x-direction only, $k_y = 0$, and $k_x = \omega/c$. it follows that the reflection $R = 0$, which means that the one-way wave equation absorbs the outgoing wave perfectly.

The Higdon's ABC, which is a representative analytically derived ABC [14], is developed based on one-way wave equation.

The N^{th} order Higdon's ABC is given as

$$B_N U = \prod_{i=1}^{N} (\partial_x + \frac{\cos\phi_i}{c}\partial_t)U = 0, \qquad i = 1,2,...,N \tag{6}$$

where, B_N denotes the N^{th} order boundary operator, ϕ_i is the incident angle which the propagating wave impinge the boundary. Obviously, when the incident angle is 0°, which means the wave is incident normal to the truncated boundary, the first order Higdon's ABC reduces to the one-way wave equation.

In the open-region simulations, suppose we have a two-dimensional computational boundary at $x=a$, the fields at any point to the left of the boundary can be expressed as

$$U = e^{j\omega t - jk_x x - jk_y y} + R\ e^{j\omega t + jk_x x - jk_y y} \tag{7}$$

where, ω is the radian frequency, R is the reflection coefficient and it expresses the amplitude of the reflected wave relative to the amplitude of the incident wave. k_x, and k_y are the wave numbers in x and y directions respectively. Ideally we would like to have zero reflection from the computational boundaries. Therefore, the spurious reflection that is induced by the imperfect absorption of the computational wall is given by the second term in (4),

$$R\ e^{j\omega t + jk_x x - jk_y y} \tag{8}$$

By simple substitution of (4) into the Higdon's ABC, the reflection coefficient R can be found

$$R[B_N] = -\prod_{i=1}^{N} \frac{-jk_x + j\cos\phi_i k}{jk_x + j\cos\phi_i k} \qquad (9).$$

I.3.2 Numerically Derived Absorbing Boundary Conditions

Another important category of ABC is the numerically derived ABC. Examples in this category are the Liao's and Colonius ABCs [20], [21]. The numerically derived ABCs are constructed by using the extrapolation of the numerical fields in both space and time. In numerically derived ABC, the boundary nodes are denoted as a linear combination of the interior nodes as long as the reflection generated by the boundary can be much less than the incident wave. As illustrated in Fig. 3, the boundary nodal value at current time t, $U(m,n,t)$ is constructed from the linear combination of numerical fields, $U(m-i,n-j,t)$, $U(m-i,n-j,t-\Delta t)$,…, $i,j=1,2,3$…in both space and time.

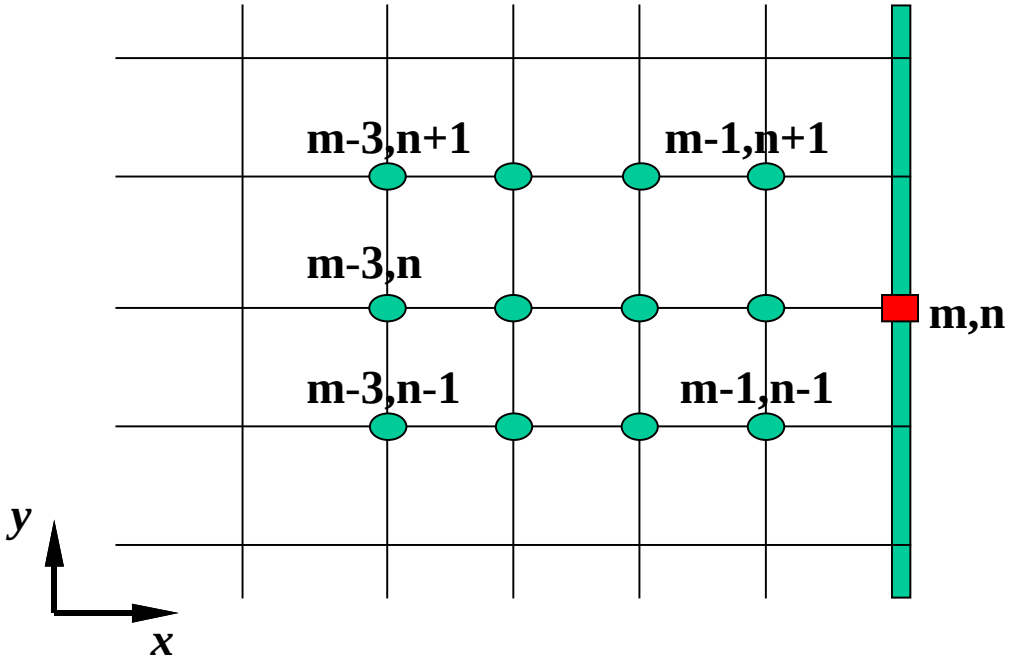

Fig. 3. Illustration of the construction of numerically derived ABCs.

Consider a mesh-truncation boundary parallel to the *y*-axis and located at $x=x_0$. We denote the field at a point in a two-dimensional computational domain as $u^l_{m,n}$, where

$$u^l_{m,n} \equiv u^{l\Delta t}_{m\Delta x, n\Delta y} \tag{10}$$

Therefore, using a numerically derived ABC, the fields at the boundary nodes can be written as

$$u^l_{m,n} = \sum_{i=-I}^{I} \sum_{j=-J}^{J} \sum_{k=1}^{l} \beta_{ijk} u^k_{i,j} \tag{11}$$

where β_{ijk} are constant coefficients. The reflection generated by the numerically derived ABCs can be derived similar to the derivation of the reflection for analytically derived ABCs. In the two-dimensional numerical domain, the field

$$u^l_{m,n} = e^{j\omega l\Delta t - jk_x m\Delta x - jk_y n\Delta y} + R_d \; e^{j\omega l\Delta t + jk_x m\Delta x - jk_y n\Delta y} \tag{12}$$

substituting this field into (11), the reflection constant R_d can be found, which is a function of (Δx,Δt).

I.4 OUTLINE OF THESIS

The research work presented in this thesis addresses three areas: 1) developing C-COM operators on numerically derived ABCs in FDTD, 2) developing C-COM operators on ABCs in frequency domain numerical techniques, and 3) developing accurate stability analysis scheme for analytically derived ABCs.

In chapter 1, the theory of complementary operators is briefly described. The COM operators for both analytically derived ABCs and for numerically derived ABCs are developed. The COM operators for frequency domain numerical techniques are also introduced. The C-COM implementation in both time domain and frequency domain numerical techniques is also developed.

In chapter 2, the applications of C-COM in open-region electromagnetic simulations are investigated. The applications of C-COM in this thesis include the applications on the numerically derived ABC in FDTD and the typical ABC in frequency domain using both Finite Difference and Finite Element techniques. Comparison study between the Perfectly Matched Layer (PML) method and C-COM is performed on radiation problems and waveguide problems.

Earlier works on stability issues resulted from ABCs were not inclusive. Some inconsistence was observed in earlier publications [22]-[27]. In this work, a coupled stability analysis method based on the stability analysis of linear time invariant (LTI) system in digital signal processing is developed. In chapter 4, the coupled stability

analysis is discussed and applied to Higdon's ABC in FDTD. The results using this novel stability analysis method are consistent with the phenomena observed in numerical experiments. Within the framework of stability, the effects of weighting functions in the finite difference scheme are investigated in chapter 5.

II. COMPLEMENTARY OPERATORS FOR ABSORBING BOUNDARY CONDITIONS

II.1 THEORY

In 1995, Ramahi introduced the complementary operators method (COM) as a simple, flexible and efficient technique for mesh truncation in FDTD simulation. The original COM is developed based on Higdon's ABC [16]. The COM operators were also extended to the general analytical ABCs in FDTD. The COM operators, are two independent operators conducted on the existing absorbing boundary conditions to annihilate the first order and odd-order reflections.

The idea of the COM operators is to annihilate the reflection arise from existing absorbing boundary conditions [16]. If with such a pair, two operations on an absorbing boundary condition can generate reflection R and $-R$, which are equal in magnitude but 180 degree out of phase, then the average of the solutions resulted from two operations will have a perfect absorption of an outgoing wave. However, the two independent solutions have multi-reflections from the absorbing boundary. Consequently, only the first order reflection, which generated by the ABC, is expected to be suppressed successfully. The complementary operations are illustrated in Fig. 4.

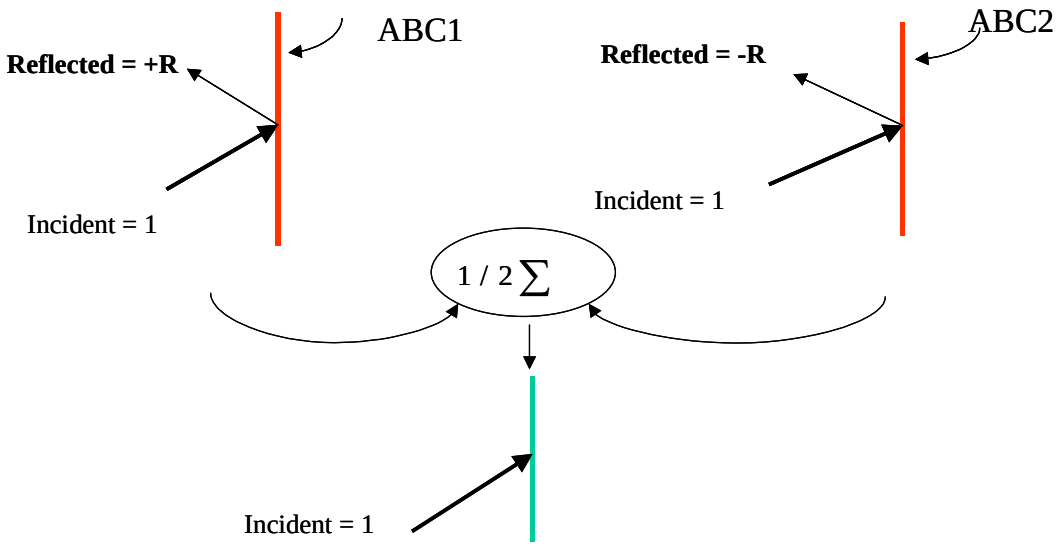

Fig. 4. Illustration of complementary operation.

II.2 COMPLEMENTARY OPERATORS METHOD (COM) IN FINITE DIFFERENCE TIME-DOMAIN

II.2.1 Complementary Operators for Analytically Derived ABC

A generalized Higdon's ABC is a representative analytically derived ABC [7],

$$B_N U = \prod_{i=1}^{N} (\partial_x + \frac{\cos\phi_i}{c}\partial_t)U = 0 \qquad (1)$$

An operation pair, the space derivative and the time derivative, (∂x, ∂t), reported in [16], is used to generate complementary solutions. Applying the complementary operator pair (∂_x, ∂_t) to the Higdon's ABC, we obtain two separate boundary conditions

$$B_N^- U = \partial_x \prod_{i=1}^{N-1} (\partial_x + \frac{\cos\phi_i}{c}\partial_t)U = 0 \qquad (2)$$

and,

$$B_N^+ U = \partial_t \prod_{i=1}^{N-1} (\partial_x + \frac{\cos\phi_i}{c}\partial_t) U = 0 \tag{3}$$

where B_N^- and B_N^+ denotes the complementary operation of the Higdon's ABC with the complementary operator pair. The field, U is subject to a two-way propagation wave, in two-dimensional space, let

$$U = (e^{j\omega t - jk_x x} + R\ e^{j\omega t + jk_x x}) e^{-jk_y y} \tag{4}$$

in which, ω is the radian frequency, R is the reflection coefficient, and k_x,k_y are the wave numbers in x, y directions, respectively. Substituting the field U into the complementary pairs, we have the reflections of the two complementary operations

$$R[B_N^-] = (+1)\prod_{i=1}^{N-1} \frac{-jk_x + j\cos\phi_i k}{jk_x + j\cos\phi_i k} \tag{5}$$

and,

$$R[B_N^+] = (-1)\prod_{i=1}^{N-1} \frac{-jk_x + j\cos\phi_i k}{jk_x + j\cos\phi_i k} \tag{6}$$

Obviously, the average of the two reflections cancels the primary reflection arises from the original Higdon's ABC. Therefore, the complementary pairs generate two complementary boundary conditions. The average of the two solutions using these complementary boundary conditions cancels the primary reflection generated by the original boundary condition.

II.2.2 Complementary Operators for Numerically Derived ABC

Numerically derived ABCs use extrapolation method to solve the boundary unknowns based on the numerical fields in the interior computational domain. Consider a

mesh-truncation boundary parallel to the *y*-axis and located at $x=x_0$. When implemented in an FDTD scheme, any numerically-derived ABCs enforced at $x= x_0$ can be expressed as a weighted polynomial of space- and time-shift operators as [28]:

$$BU = \left(-I + \sum_{i=-I}^{I} \sum_{j=-J}^{J} \sum_{k=1}^{K} \beta_{ijk} S_x^{-i} S_y^{-j} T^{-k} \right) U = 0 \tag{7}$$

Where U is the unknown field, and β_{ijk} are constant coefficients. I is the identity operator, S_x^{-i} is the space-shift operator along the *x*-axis, S_y^{-i} is the space-shift operator along the *y*-axis, and T^i is the time-shift operator. The shift operators are explicitly expressed as follows:

$$\begin{aligned}
&IU(t=N, x=a, y=b) = U(t=N, x=a, y=b) \\
&T^{-i}U(t=N, x=a, y=b) = U(t=N-i\Delta t, x=a, y=b) \\
&S_x^{-i}U(t=N, x=a, y=b) = U(t=N, x=a-i\Delta x, y=b) \\
&S_y^{-i}U(t=N, x=a, y=b) = U(t=N, x=a, y=b-i\Delta y)
\end{aligned}$$

where Δx and Δy are the mesh spacing in *x* and *y* direction, respectively, and Δt is the time step. Equation (7) simply expresses the relationship between the field, *U*, at the boundary node in terms of interior nodes.

The essential two operators in C-COM are ∂_x and ∂_t. In an FDTD scheme, these two operators are converted to the following discrete operators:

$$\partial_x \rightarrow \left(\frac{I - S^{-1}}{\Delta x} \right) \left(\frac{I + T^{-1}}{2} \right) \tag{8}$$

and

$$\partial_t \rightarrow \left(\frac{I - T^{-1}}{\Delta t} \right) \left(\frac{I + S^{-1}}{2} \right) \tag{9}$$

Notice that the second term in each expression constitutes an averaging process that is essential to insure both full complementariness and stability [16].

When applying the C-COM operators to the numerical boundary operator in (7), we obtain the new complementary absorbing boundary condition pair

$$B_N^- = \left(\frac{I - S^{-1}}{\Delta x}\right)\left(\frac{I + T^{-1}}{2}\right)B \tag{10}$$

and

$$B_N^+ = \left(\frac{I - T^{-1}}{\Delta t}\right)\left(\frac{I + S^{-1}}{2}\right)B \tag{11}$$

A time-harmonic plane wave incident on the boundary at $x=x_0$ will experience a reflection from the terminal boundary. The field due to the incident wave for $x < x_0$ can be expressed as

$$U_\Delta = e^{-jk_x n_x \Delta_x - jk_y n_y \Delta_y + j\omega n_t \Delta_t} + R_d\, e^{jk_x n_x \Delta_x - jk_y n_y \Delta_y + j\omega n_t \Delta_t} \tag{12}$$

The field U_Δ, is defined at discrete points in space, $x=n_x\Delta_x$, $y=n_y\Delta_y$, and the discrete points in time, $t=n_t\Delta_t$. k_x, and k_y are the wave number in x, and y direction, respectively, ω is the radian frequency, and R_d is the reflection coefficient.

Applying (10) and (11) to (12), and assuming that the reflection coefficient of the numerical absorbing boundary operator B is $R[B]$, we obtain the following two reflection coefficients:

$$R_d[B_N^- U] = -e^{jk_x\Delta_x} R[B] \tag{13}$$

and

$$R_d[B_N^+ U] = e^{jk_x\Delta_x} R[B] \tag{14}$$

Notice that irrespective of whether the boundary operator is analytically-derived or numerically-derived, the application of the complementary operators resulted in reflections coefficients that are precisely 180^o out of phase, hence insuring full complementariness.

II.3 COMPLEMENTARY OPERATORS IN TIME-HARMONIC COMPUTATIONAL SIMULATIONS

In time-harmonic computational electromagnetics, finite difference and finite element method both are popular numerical techniques. The complementary operators in time-harmonic computational electromagnetics are based on finite-difference operations.

Consider a computational domain terminated at $x=x_0$, a finite-difference operator pair, $D_x^- = I - S^{-1}$, $D_x^+ = I + S^{-1}$, operates on a frequency-domain absorbing boundary operator B [28],

$$D_x^- BU = (I - S^{-1})B\,U = 0 \tag{15}$$

and,

$$D_x^+ BU = (I + S^{-1})B\,U = 0 \tag{16}$$

The corresponding reflection coefficients can be derived

$$R[D_x^- B] = -e^{jk_x\Delta_x} R[B] \tag{17}$$

$$R[D_x^+ B] = e^{jk_x\Delta_x} R[B] \tag{18}$$

in which, $R[B]$ is the reflection coefficient of the original absorbing boundary operator applied to, and k_x is the wave number in the x-direction. Notice that $R[D_x^+ B]$ and

$R[D_x^- B]$ are precisely 180 degrees out of phase and, hence full complementariness is achieved analytically and numerically.

II.4 THEORY OF CONCURRENT COMPLEMENTARY OPERATORS METHOD

Since the COM operation requires two independent operations, this needs more computer resources and CPU time than the regular absorbing boundary conditions. The concurrent complementary operators method (C-COM), which makes the two independent complementary operations done on a periphery in the computational domain, was developed to take advantage the superb absorption of the COM method and avoid the additional computation [17]. With the concurrent version of COM, not only the first order reflection can be annihilated, but also the higher order multi-reflection can be suppressed, as illustrated in Fig. 5. By averaging the fields at the interface between the boundary zone and the interior region, the final reflections entering the interior region are of the second order of the original reflections.

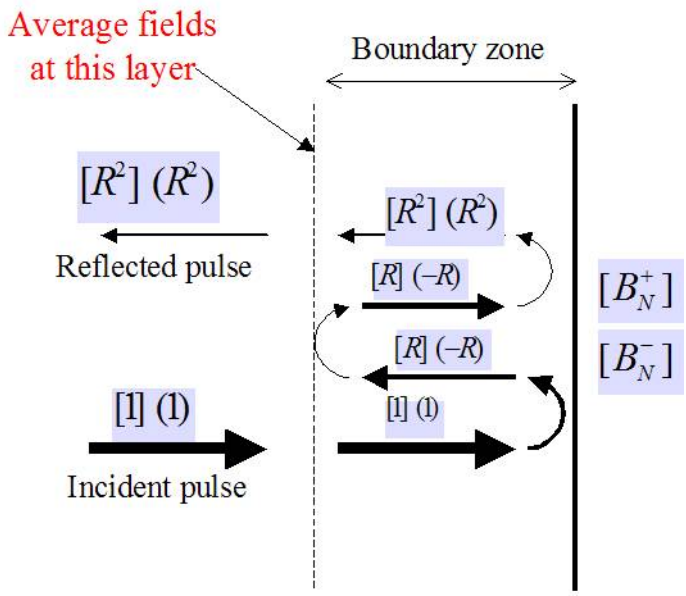

Fig. 5. Illustration of the reflection resulted from C-COM operation.

II.4.1 C-COM Implementation in Transient Simulations

When implementing C-COM in FDTD method, we first divide the computational domain into two regions: a boundary zone and an interior region, as shown in Fig. 6. The interior region includes the simulated structure and any localized sources.

To reduce the side boundary reflections, in the boundary zone, instead of defining one storage location for each field component, we allocate two storage (memory) locations to each field component. Then, a single simulation of the problem is performed in the interior region, and stored. Within the boundary zone, the field components are stored in two arrays independently. Next, we apply the two complementary boundary operators to two stored boundary zone field sets, respectively. Notice that each set of fields in the boundary zone is updated independently of the other set. This amounts to having two independent simulations in the boundary zone.

The next step is to connect the solutions in the interior zone and boundary zone. This is performed by averaging the two values obtained for each field at the interface lying between the interior zone and boundary zone. The distance from the interface to the boundary has to be at least the width (size) of the stencil, which is essential for the discretization of the ABC.

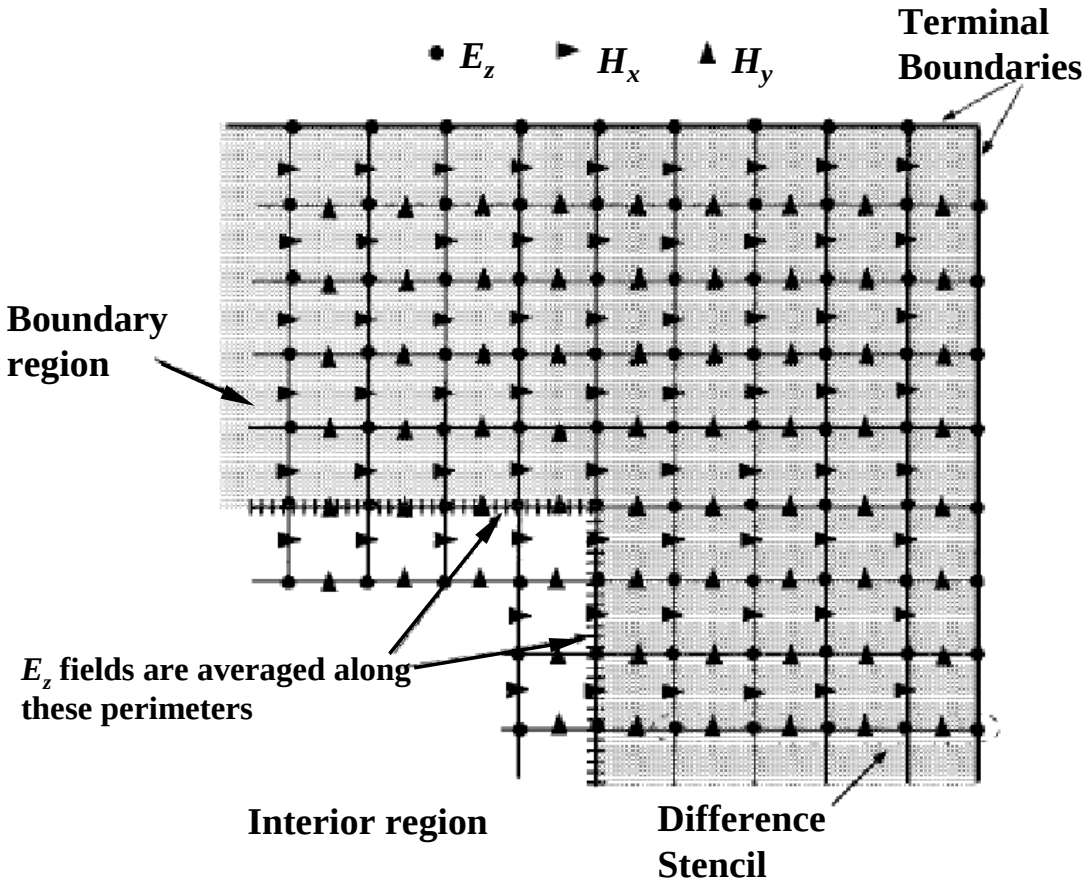

Fig. 6. Illustration of implementation of C-COM in FDTD.

The above steps required for implementation of the C-COM for a two-dimensional TM case can be summarized as following:

1) E_z, H_x, and H_y are updated in the interior region according to standard FDTD schemes.
2) On the mesh terminal boundary, apply BN- on $E_z^{(1)}$ and B_N^+ on $E_z^{(2)}$.
3) Within the boundary layer, $E_z^{(1)}$ is updated from $H_x^{(1)}$, and $H_y^{(1)}$, and $E_z^{(2)}$ is updated from $H_x^{(1)}$ and $H_y^{(1)}$. Both sets are updated using standard FDFD schemes.
4) $E_z^{(1)}$ and $E_z^{(2)}$ are averaged along the interface connecting the two regions, (see Fig. 6). The new values of $E_z^{(1)}$ and $E_z^{(2)}$ along the interface are given the value of the average $(E_z^{(1)}+ E_z^{(2)})/2$.
5) Advance time by one-half time step.
6) Update H_x and H_y in the interior region. At the interface, H_x and H_y in the interior region will use $(E_z^{(1)}+ E_z^{(2)})/2$ as calculated in step 4.
7) In the boundary layer, $H_x^{(1)}$ and $H_y^{(1)}$ are updated using $E_z^{(2)}$.

The procedure outlined above annihilates reflections arising from side boundaries. To extend the annihilation to corner reflections, four storage locations need to be assigned to each field in the boundary zone to account for secondary reflections. Then an identical averaging procedure to the one outlined above is performed, except having four field values to update the in the boundary zone and four field values to average at the interface.

II.4.2 C-COM Implementation in Time-Harmonic Simulations

The implementation of C-COM in frequency-domain numerical simulation is of a great difference, comparing with that of C-COM in time-domain. In time-harmonic numerical techniques, we solving a steady state electromagnetic problem rather than a time dependent problem, therefore, a matrix system, resulted from the time-harmonic equations (Helmholtz equations) is developed to characterize the problem. As an example, we illustrate the C-COM implementation in a two-dimensional TM problem.

The first step in the implementation of the time-harmonic numerical techniques is to divide the computational region into grid. Following a procedure highly similar to that used in the implementation of the C-COM in time-domain simulation, we divide the computational domain (grid) into two non-overlapping regions—a boundary region and an interior region as shown in Fig. 7. The interior region includes all radiating or scattering objects, while the boundary region is an empty domain set up purely for computational purposes. To each field node in the boundary region we assign two field values, E_z^1 and E_z^2. In the interior region we assign a single field value, E_z to each node, as in conventional implementation.

Next, we apply either frequency domain numerical techniques to each node in the interior region as in standard implementation. In the boundary region, we apply the numerical techniques to each set of fields designated by the superscripts *1* and *2*.

The next step is the implementation of the complementary operators. The first operator D_x^- is applied to the set of fields denoted by E_z^1 whereas the second operator D_x^+ is applied to the second set of fields denoted by E_z^2.

The final step links the boundary and interior regions. This is accomplished by constructing an interface between the two regions. On the interface, the field values needed from the boundary region are obtained from the average values of E_z^1 and E_z^2. Let Γ be the interface perimeter between the boundary layer and the interior region. (The interior region is inclusive of Γ.) Let us focus on the left-hand-side segment of Γ shown in Fig. 7. On Γ, the update equation for the fields uses the average field values $(E_z^1 + E_z^2)/2$ from the left-hand side and E_z from the interior region. The averaging is processed by modifying the coefficients of the matrix system by replacing the corresponding coefficients of E_z^1 and E_z^2 so that the average of the two fields are obtained through the modified equations.

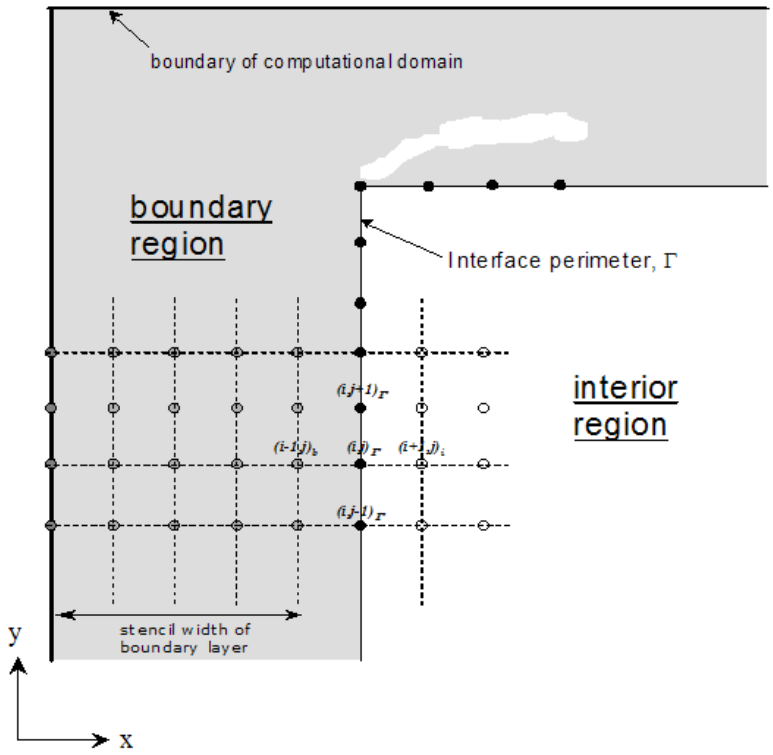

Fig. 7. Illustration of C-COM implementation using finite difference frequency domain method.

II.5 CONCLUSIONS

In this chapter, the complementary operators method theory and its concurrent version for analytically derived absorbing boundary conditions (ABCs) in time-domain open-region simulations are introduced. The C-COM theory is extended for numerically derived ABCs in time-domain simulations. The C-COM theory and implementation for time-harmonic numerical techniques are developed.

III. APPLICATION OF C-COM IN OPEN-REGION RADIATION AND SCATTERING PROBLEMS

In this chapter, the C-COM applications in open-region electromagnetic simulations are developed. The C-COM operators for Liao's ABC in FDTD, the C-COM for Bayliss-Turkel ABC in both FDFD and FEM are presented. Comparison study between C-COM and PML in frequency domain method is also presented.

III.1 C-COM ON LIAO'S ABC IN FINITE DIFFERENCE TIME-DOMAIN

As discussed in chapter 1, the Liao's ABC is a typical numerically derived ABC, based on the extrapolation of the wave fields in space and time using Newton backward-difference polynomial. The Liao's ABC at the boundary $x=x_0$, is given as [21]

$$U(t+\Delta t, x_0) = \sum_{j=1}^{N} (-1)^{j+1} C_j^N U(t-(j-1)\Delta t, x_0 - j\alpha c\ \Delta t) \qquad (1)$$

where c is the speed of light, α is a constant in the range $0.5<\alpha<2$, the binomial coefficient C_j^N is

$$C_j^N = \frac{N!}{(N-j)!} \qquad (2)$$

Converting (1) to a generalized numerically derived ABC form, Liao's ABC reduces to:

$$B_L^N U = (-I + \sum_{i=1}^{N}\sum_{j=1}^{M} \beta_{ij} T^{-i} S^{-j}) U = 0 \qquad (3)$$

where β_{ij} are constant coefficients, and *N,M* is the order of the operator.

Applying the complementary operators on (3), we have:

$$\left(\frac{I-S^{-1}}{\Delta x}\right)\left(\frac{I+T^{-1}}{2}\right)B_L^N U = 0 \qquad (4)$$

and

$$\left(\frac{I-T^{-1}}{\Delta t}\right)\left(\frac{I+S^{-1}}{2}\right)B_L^N U = 0 \qquad (5)$$

To demonstrate the validity of the above implementation, we present a numerical experiment where the C-COM is applied to Liao's 2nd and 3rd order ABCs. (This procedure will be referred to as C-COM(Liao2) and C-COM(Liao3).) We consider the problem of a current source radiating in a two-dimensional free space (TM polarization). The size of the computational space is 31Δx x 31Δy. For simplicity, we consider a uniform mesh in the *x* and the *y* directions, with a space step $\Delta x = \Delta y = \Delta s = 0.015$m and time step $0.9\Delta t_c$, where Δt_c is the Courant limit. The source is located at the center point (16Δx,16Δy). The temporal form of the source is a compact pulse given by the convolution $h(t) * h(t)$, where $h(t)$ is defined as:

$$h(t) = \begin{cases} \pi 10^4 (15\sin(\omega_1 t) - 12\sin(\omega_2 t) + 3\sin(\omega_3 t)) & 0 \le t \le \tau \\ 0 & otherwise \end{cases} \qquad (6)$$

where, $\tau = 10^{-9}$, $\omega_i = 2\pi i / \tau, i = 1,2,3, \ldots$

An observing point is chosen at (19Δx,19Δy). The C-COM averaging layer perimeter is positioned 10 cells from the mesh terminal boundaries in all directions.

Fig. 8 shows the normalized error at the observation point when using Liao 2nd, Liao 3rd, C-COM(Liao2), and C-COM(Liao3). The normalized error is defined as

$$error = \log \left| \frac{E_{abc} - E_{ref}}{\max(E_{ref})} \right|$$

where E_{abc} is the solution obtained using the different boundary condition schemes and E_{ref} is the reference numerical solution obtained devoid of any boundary reflections. From Fig. 8, we observe that the C-COM operation resulted in a significant reduction in the reflected field. In fact, since the pulse energy is confined to a support not exceeding 100 time steps, we observe an effective reduction in the reflected pulse of several orders of magnitude. Additional key observation is the stability of the solutions. For the case of C-COM(Liao3), the simulation was run for 100,000 time steps and the solution did not exhibit any instable behavior, as shown in Fig. 9. Equally encouraging is the fact that the simulation did not generate any instability from the corner region, which is known to induce catastrophic instabilities [27]. This stable behavior is in sharp contrast to the case when C-COM is applied on analytic ABCs such as Higdon's operators [27].

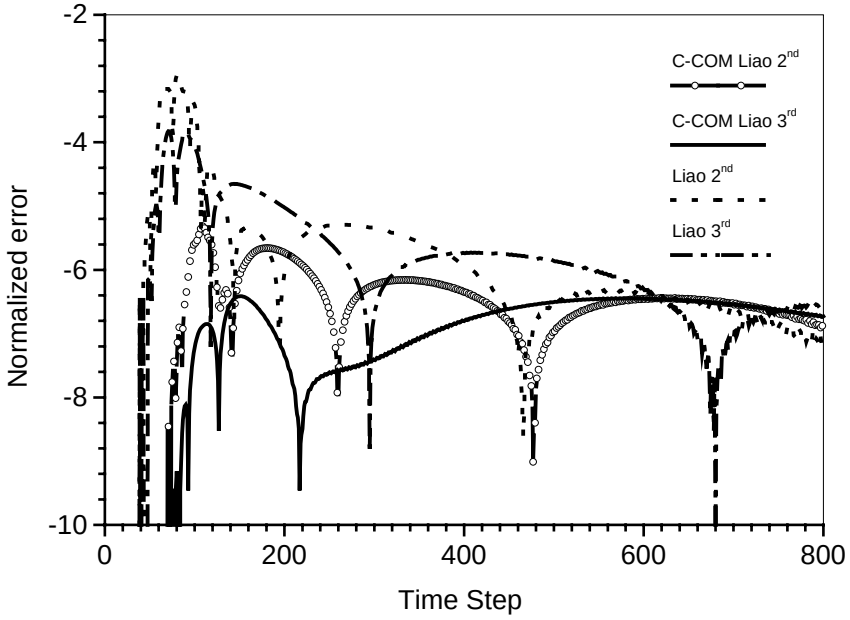

Fig. 8. Comparison of the error of C-COM on Liao's 2nd and 3rd order ABC.

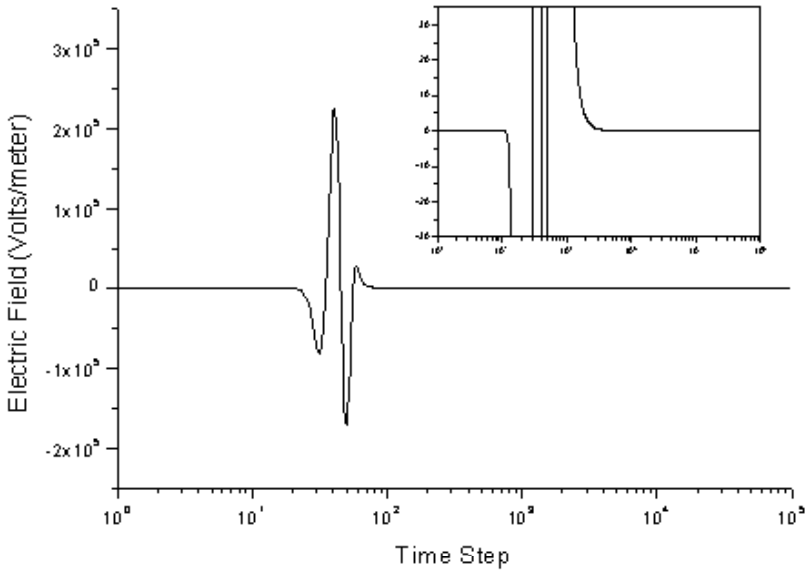

Fig. 9. Stabile behavior of the FDTD simulation with C-COM(Liao3).

III.2 C-COM IN FINITE DIFFERENCE FREQUENCY-DOMAIN

Although the time-domain and frequency-domain simulations are two different mathematical representations of the same physical phenomenon, the numerical solution paradigm could be totally different. Therefore, the complementary operator pair in time-domain needs to be adapted to fit the particular numerical techniques in frequency-domain.

A. C-COM on Bayliss-Turkel ABC in Finite Difference Frequency-Domain

In a two dimensional time-harmonic computational electromagnetic problem, the governing equation is the Helmholtz wave equation, which, for the case of TM-polarization is given by

$$\nabla^2 E_z + k^2 E_z = 0 \qquad (7)$$

where k is the wave number. (For the case of TE-polarization, E_z is replaced by H_z.) The field E_z corresponds to the scattered or total field. (The physical boundary conditions pertaining to the scattering object will be adjusted in accordance with the formulation used.)

The basic idea of Bayliss-Turkel ABC is to construct a weighted sum of three partial derivatives of the field: 1) a spatial partial derivative in the direction of outgoing wave propagation, 2) a spatial partial derivative in a direction transverse to the direction of outgoing wave propagation, and 3) a time partial derivative. Properly constructed, this differential boundary operator systematically annihilates an outgoing scattered wave, leaving a remainder term that represents the residual error of the process. Consider

solutions $U(R,\theta,\phi,t)$ in a spherical coordinates system, forming a partial derivative operator based on one-way wave equation,

$$L = \frac{1}{c}\frac{\partial}{\partial t} + \frac{\partial}{\partial R} \tag{8}$$

The first-order Bayliss-Turkel boundary operator is given as

$$B_1 = L + \frac{1}{R} \tag{9}$$

and the remainder (error) of the first-order boundary operator is $O(R^{-3})$. The N^{th} Bayliss-Turkel boundary operator can be obtained via a recursion relation:

$$B_N = (L + \frac{2N-1}{R})B_{N-1} \tag{10}$$

The remainder term is $O(R^{-2N-1})$.

For a planar (Cartesian) boundary, the N^{th} order BT operator in frequency domain for a planar boundary is reduced to a Higdon's ABC

$$B_N = (\partial_n + jk)^N \tag{11}$$

where ∂_n is the partial derivative of the field in the direction normal to the computational boundary. When the outer boundary is planar and coinciding with the Cartesian planes, the BT condition reduces to Higdon's boundary condition when it is applied in the frequency domain.

Applying the FDFD scheme to the free-space Helmholtz equation at an interior node $(i, j)_i$, we have

$$E_z(i-1, j)_i + E_z(i+1, j)_i + E_z(i, j+1)_i + E_z(i, j-1)_i + (k^2\Delta^2 - 4)E_z(i, j)_i = 0 \tag{12}$$

In the boundary region, we apply the finite-difference equation to each set of fields designated by the superscripts *1* and *2*, we have

$$E_z^1(i-1,\, j)_b + E_z^1(i+1,\, j)_b + E_z^1(i,\, j+1)_b + E_z^1(i,\, j-1)_b + \left(k^2\Delta^2 - 4\right)E_z^1(i,\, j)_b = 0 \tag{13}$$

$$E_z^2(i-1,\, j)_b + E_z^2(i+1,\, j)_b + E_z^2(i,\, j+1)_b + E_z^2(i,\, j-1)_b + \left(k^2\Delta^2 - 4\right)E_z^2(i,\, j)_b = 0 \tag{14}$$

The next step is the implementation of the complementary operators. The first operator $D_x^+ = I + S^{-1}$ is applied to the set of fields denoted by E_z^1 whereas the second operator $D_x^- = I - S^{-1}$ is applied to the second set of fields denoted by E_z^2. More explicitly, we have

$$\{D_x^+ B\}E_z^1 = 0 \tag{15}$$

$$\{D_x^- B\}E_z^2 = 0 \tag{16}$$

The final step links the boundary and interior regions. This is accomplished by constructing an interface between the two regions. On the interface, the field values needed from the boundary region for the FDFD equation are obtained from the average values of E_z^1 and E_z^2. Let Γ be the interface perimeter between the boundary layer and the interior region. (The interior region is inclusive of Γ.) On Γ, the update equation for the fields uses the average field values $(E_z^1 + E_z^2)/2$ from the left-hand side and E_z from the interior region. Thus, the finite difference equation for the fields on Γ is given by

$$\frac{1}{2}\left\{E_z^1(i-1,\, j)_b + E_z^2(i-1,\, j)_b\right\} + E_z(i+1,\, j)_i + E_z(i,\, j+1)_\Gamma + E_z(i,\, j-1)_\Gamma + \left(k^2\Delta^2 - 4\right)E_z(i,\, j)_\Gamma = 0$$

(17)

Similar equations are applied on the other three sides of Γ. The FDFD equations for the corner nodes of the interior region are slightly different. For example, the finite difference equation for the upper left-hand corner node is given by

$$\frac{1}{2}\left\{E_z^1(i-1,\, j)_b + E_z^2(i-1,\, j)_b\right\} + E_z(i+1,\, j)_\Gamma +$$
$$\frac{1}{2}\left\{E_z^1(i,\, j+1)_b + E_z^2(i,\, j+1)_b\right\} + E_z(i,\, j-1)_\Gamma + \left(k^2\Delta^2 - 4\right)E_z(i,\, j)_\Gamma = 0$$

(18)

The width of the boundary region must be greater than the width of the stencil demanded by the differential operator used in the C-COM. For instance, if *B* is a 3rd order BT operator, then the order of the C-COM operation is 4, and consequently, the width of the stencil needed will be 5. This implies that the boundary region has to be at least 6 nodes wide.

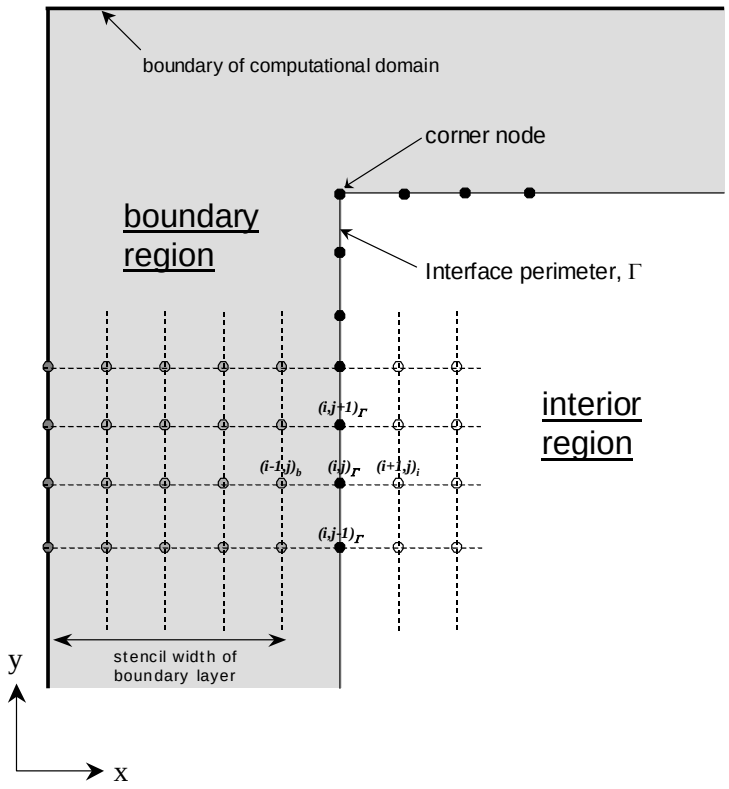

Fig. 10. The Finite-Difference Frequency-Domain grid highlighting the interior and boundary regions designated for the application of the C-COM. Also shown is the interface perimeter Γ, along which the fields from the boundary region are averaged.

To test the effectiveness of the C-COM on the absorption of outgoing waves, we consider a two-dimensional radiation problem with computational domain of 24Δ x 24Δ. (In numerical experiments given here, the grid will be uniform in the x- and y-directions with $\Delta = 0.025\lambda$.). We place a current source right at the center (12Δ, 12Δ).

Let the exact field at each of the monitor points be E^{ex}. The computed field is approximately given by $E^{c\text{-}com}$. The normalized percentage error is then given by

$$Normalized\ Error = 20log_{10}\left|\frac{E^{ex} - E^{c-com}}{E^{ex}}\right| \qquad (19)$$

The exact solution, E^{ex} is obtained from the series solution. Notice that the exact solution includes numerical errors, which are not attributed to boundary condition reflections such as numerical dispersion. Fig. 11 shows the normalized error when using C-COM4 for the radiation problem. The maximum error is –45 dB, which was observed at neighbor nodes of the current source. Due to the Bessel series characteristics, the theoretic solution is singular at the source point, therefore, the reflection observed at the neighbor nodes of the source node could be overestimated due to the space resolution, i.e., if the space step is smaller, the reflection is expect to be smaller, compared to an analytical solution obtained using series solution.

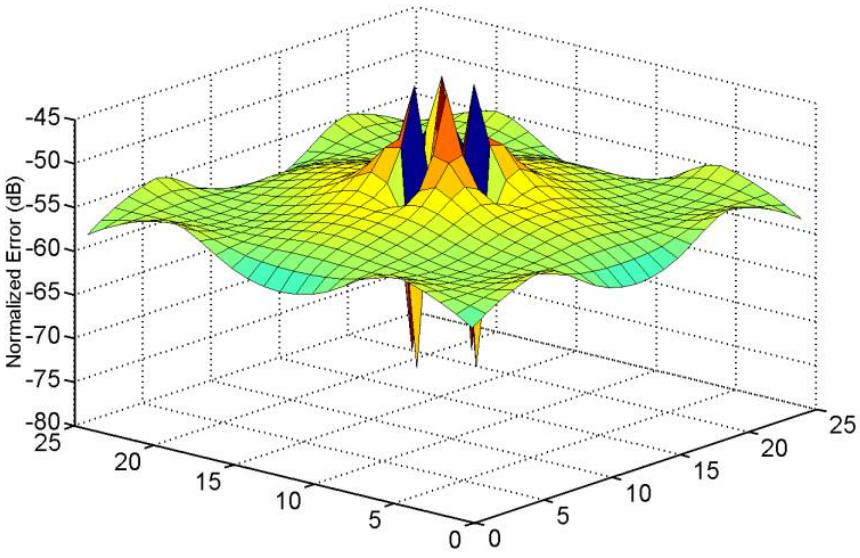

Fig. 11. Normalized error of numerical experiment using C-COM4 in FDFD.

Next, we turn to the problem of plane TM (transverse-magnetic, or E-wave) scattering by a 2.0λ x 2.0λ perfectly conducting square cylinder. The size of the computational domain is 54Δ x 54Δ. This experiment is chosen in order to study the

performance of C-COM in the shadow region of a scatterer where the scattered field has a relatively high magnitude in comparison to other regions around the scatterer. The outer boundary is positioned such that the separation between it and the conductor is 0.35λ. A total of 164 nodes span the observation contour, starting from the lower left-hand corner as shown in Fig. 12. Fig. 13 (a) and (b) show the magnitude of the scattered field on the observation contour for two different angles of incidence of ϕ=0^o and ϕ =45^o. The accuracy of the C-COM4(2,7) is observed to be quite satisfactory, especially in the shadow region of the scatterer.

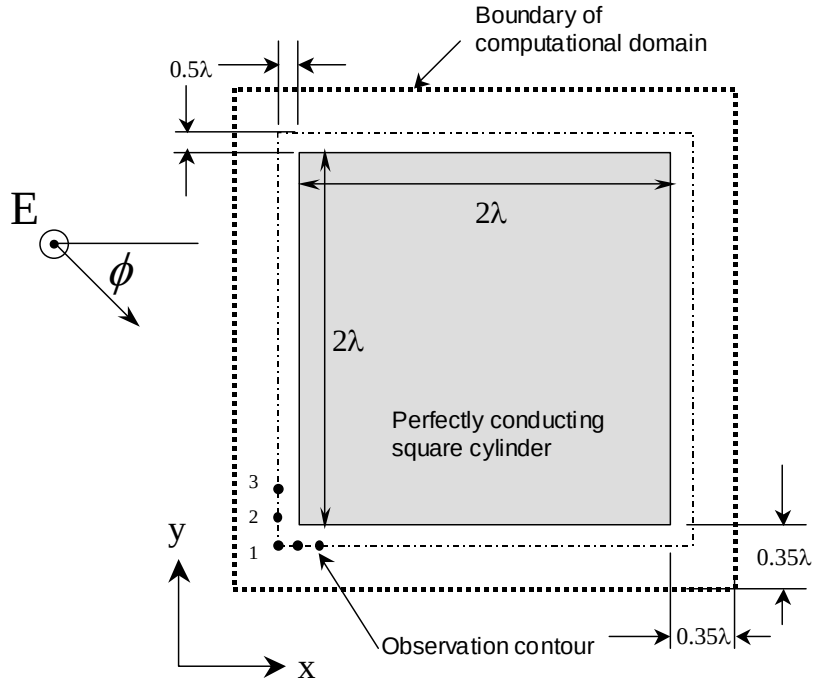

Fig. 12. Computational domain used for the problem of plane wave TM scattering from a perfectly conducting slab measuring 2.0λ x 2.0λ.

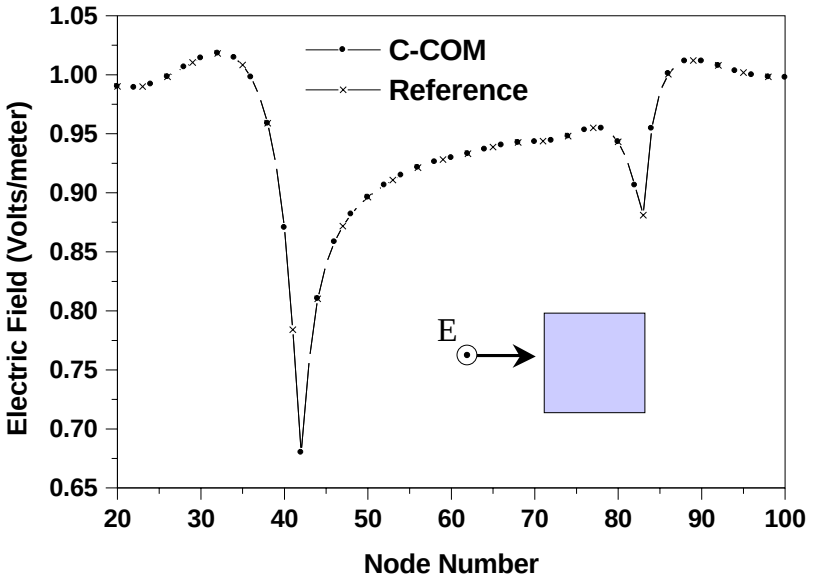

(a)

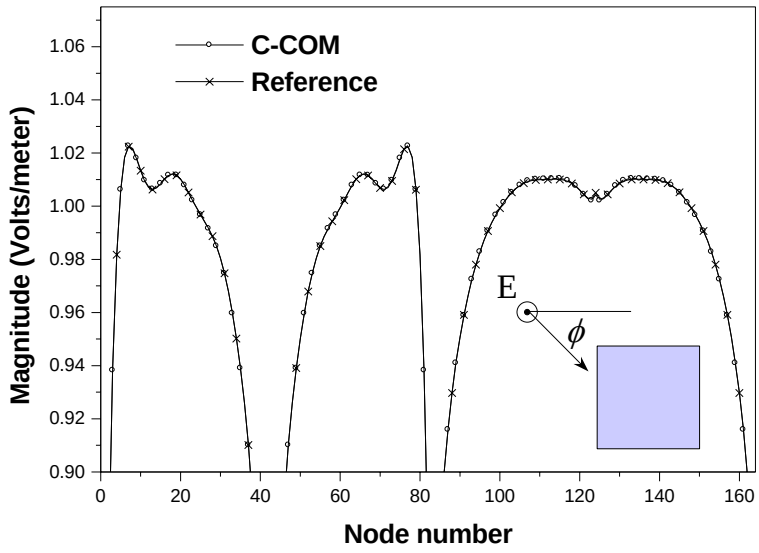

(b)

Fig. 13. Magnitude of the scattered field along Γ for the geometry shown in Fig. 4, The node numbering starts with the lower left-hand corner, as calculated using FDFD with C-COM4(2,7) (C-COM), and the reference solution (Reference), for two different angles of incidence (a) ϕ = 0.0^{o}, (b) $\phi = 45^{o}$.

For the next numerical experiment, we study the TM and TE scattering from a thin perfectly conducting rectangular slab measuring 0.2λ x 3λ. The size of the computational domain is *77*Δ x *21*Δ. The outer boundary is positioned such that the separation between it and the conductor is 0.4λ, as illustrated in Fig. 14. Fig. 15 (a) and (b) show the magnitude and phase of the scattered field due to a TM plane wave incidence. The figures show the scattered field as calculated using the C-COM method and the reference solution for comparison, at an observation contour Γ as calculated using the FDFD method with C-COM4(2,7). A total of 136 nodes span the observation contour Γ . The numbering of the nodes starts at the lower left-hand corner and proceeds clockwise. Results are only shown for field values on the upper half of the contour due to the symmetry of the solution. The results are presented for C-COM4(2,7) and the reference solution. For this and the following experiments, the reference solution is a reflection-free solution obtained when solving the problem in a domain large enough, while applying C-COM4(2,7), such that the boundary reflections are very small.

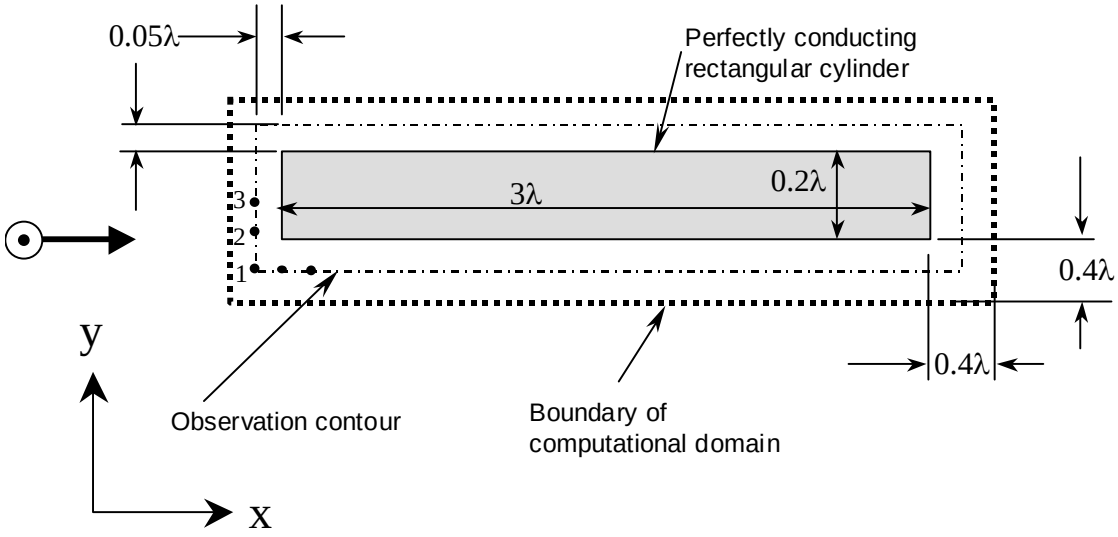

Fig. 14. Computational domain used for the problem of plane wave scattering from a perfectly conducting slab measuring 3λ x 0.2λ.

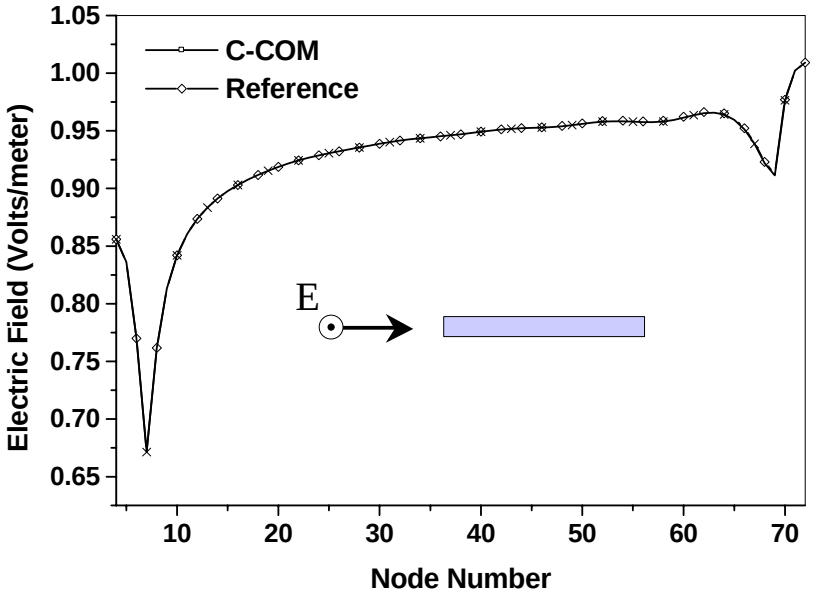

(a)

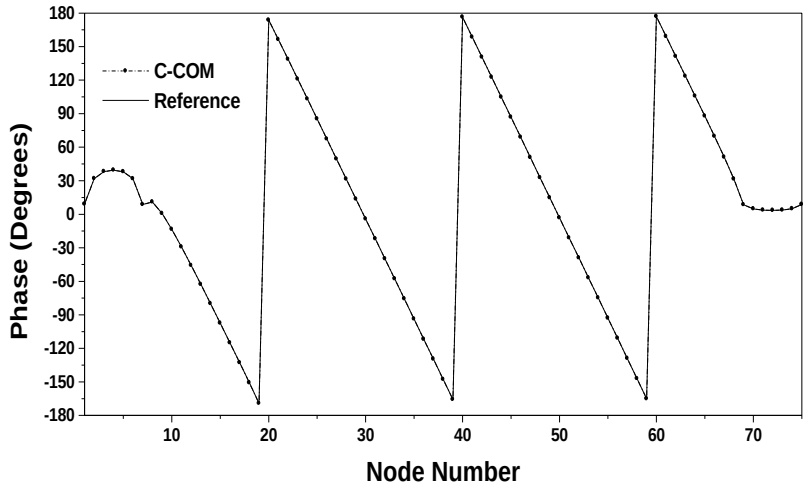

(b)

Fig. 15. Scattered field along Γ for plane wave incidence, TM-polarization (geometry shown in Fig. 4). The node numbering starts with the lower left-hand corner and proceeds clockwise. Because of symmetry, only filed points along the upper half of the contour are plotted. Field calculated using FDFD with C-COM4(2,7) (C-COM) and the reference solution (Reference) (a) Magnitude (b) Phase.

The same thin plate discussed above, measuring $0.2\lambda \times 3\lambda$, is studied under plane TE wave excitation. An identical computational geometry is used for both the scattering structure and computational domain. Unlike the results presented above where the field was plotted on an observation contour very close to the surface of the scatterer, here, we show the surface current density. Fig. 16 and Fig. 17 show the magnitude and phase of the surface current density for two different angles of incidence. Considering the close proximity of the perimeter of the computational domain from the scatterer, we observe a very strong agreement between the solution obtained using the C-COM and the reference solution. The strong performance of the C-COM solution is especially noticeable when scattered fields impinge at the computational boundary at or near-grazing incidence.

For the two perfectly conducting scatterers chosen as representative geometry, the numerical results obtained show a very strong agreement between the C-COM solution and the reference solution. Such favorable agreement is achieved despite the very close proximity of the conductor to the outer boundary. The C-COM method also demonstrates effectiveness in predicting solutions with high degree of accuracy even when the solution is dominated by waves traveling at near-grazing incidence to the terminal boundary, as was the case for the end-on incidence in TM and TE-polarization scattering.

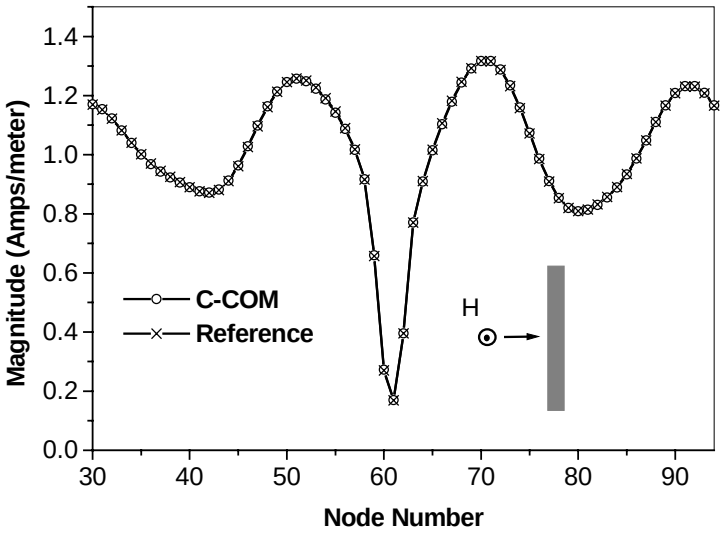

(a)

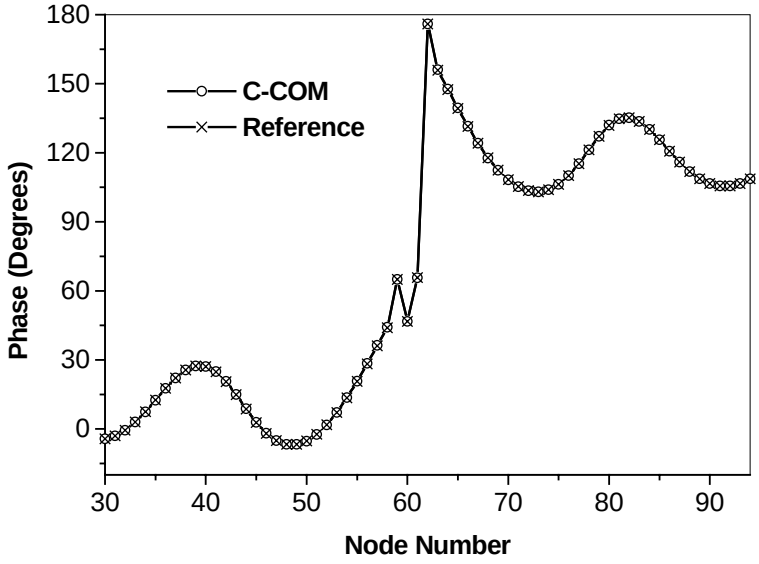

(b)

Fig. 16. Surface current density along the surface of a perfectly conducting slab for the case of broadside incidence, TE-polarization. Because of symmetry, only half of the surface span is considered. Node 30 corresponds to the middle of the left-hand-side surface. Nodes increase in number in the clockwise direction. (a) Magnitude (b) Phase.

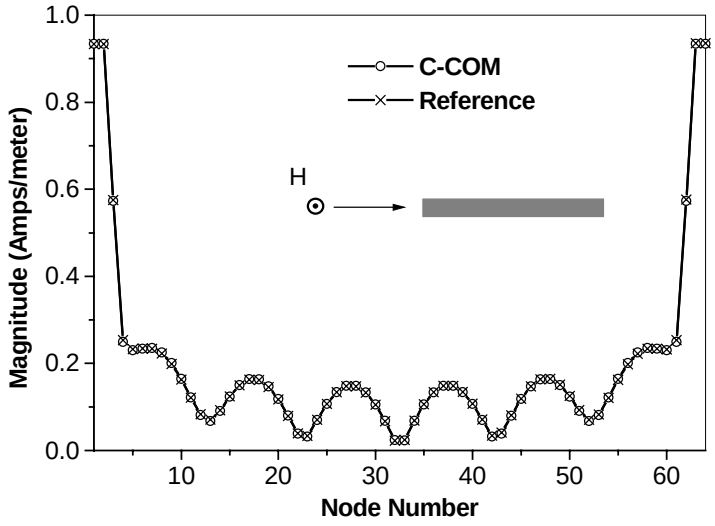

(a)

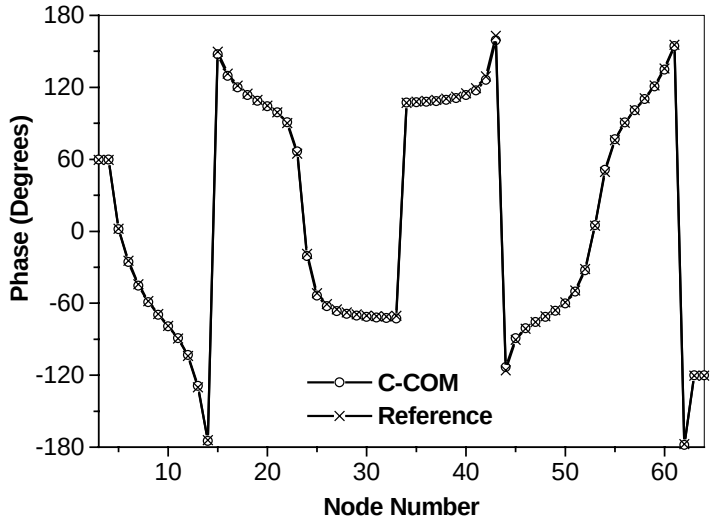

(b)

Fig. 17. Surface current density along the surface of a perfectly conducting, slab for the case of end-on incidence, TE-polarization. Because of symmetry, only half of the surface span is considered. Node 3 corresponds to the middle of the left-hand-side surface. Nodes increase in number in the clockwise direction. (a) Magnitude (b) Phase.

B. Comparison Study on C-COM and PML in Finite Difference Frequency-Domain

A comparison study between PML and C-COM is investigated in a $15\Delta \times 15\Delta$ interior computational domain, with a current source placed at the center, as illustrated in Fig. 18. The exact solution is obtained by using the series solution. The PML requires 8 layers extra. Notice that this extra requirement by the PML method means that the total computational domain size (for the PML simulation) is $38\Delta \times 38\Delta$ which is comparable to the extra memory and CPU time needed for C-COM4. The observed reflections at edges parallel to outer boundary, including the averaging interface, the first layer, the second layer and the third layer next to the averaging interface, are plotted in Fig. 19. The numerical experiments show that with C-COM4, even inside the boundary zone where the averaging takes place, the reflection is significantly reduced in comparison to the PML solution. At the same computational resource cost of PML, we can easily reach more than 10dB less reflection by using C-COM4 boundary treatment.

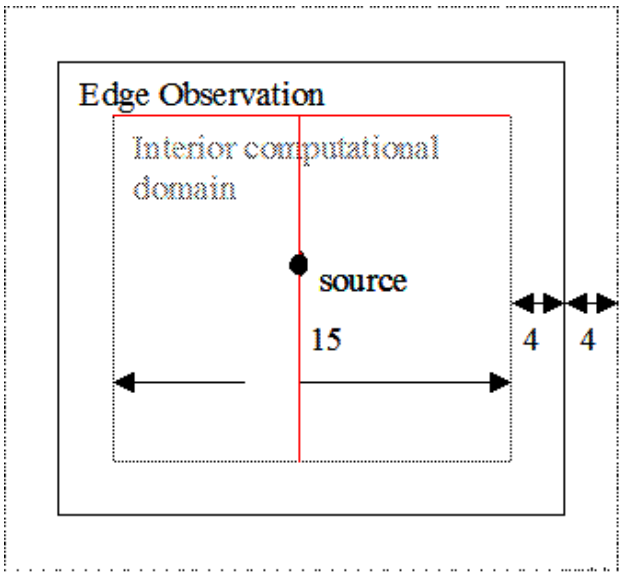

Fig. 18. A radiation problem numerical experiment.

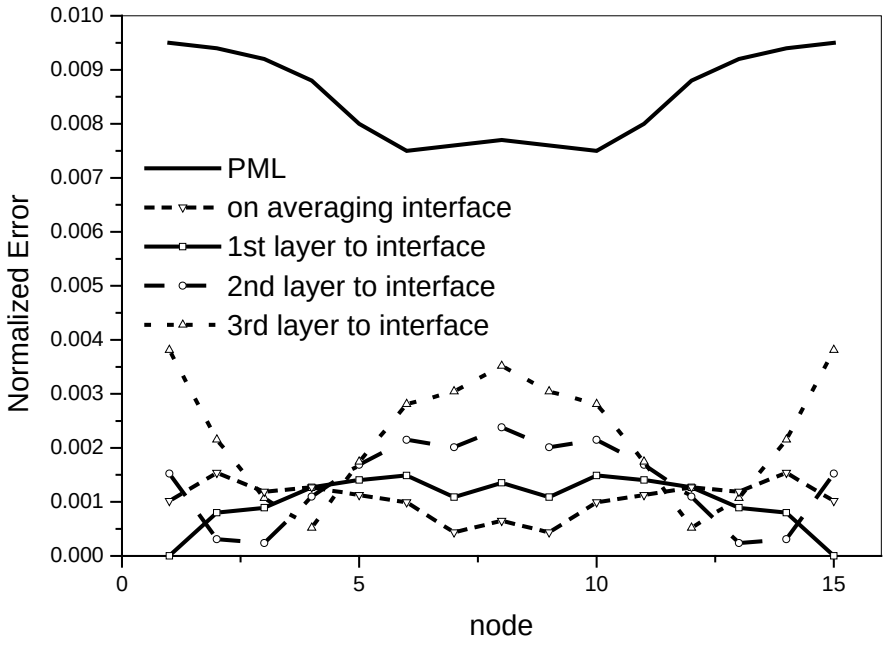

Fig. 19. Observed reflection at different locations of the numerical experiment.

III.3 C-COM IN FINITE ELEMENT METHOD

A. Application of the C-COM on Bayliss-Turkel ABC in Finite Element Method

Using finite difference scheme of Bayliss-Turkel (BT) ABC, it can be implemented in a FEM algorithm to absorb the outgoing wave [32]. This implementation of the boundary condition provides a simple and easy way to integrate the absorbing boundary conditions developed in time-domain into the time-harmonic computational electromagnetics.

For a planar (Cartesian) boundary, the N^{th} order BT operator in frequency domain is given by

$$B_N = (\partial_n + jk)^N \tag{20}$$

Using finite difference scheme, the boundary unknowns, U_b, can be expressed as a function of interior fields, U_i,

$$U_b = BU_i \tag{21}$$

The interior fields, U_i, are calculated from the finite element discretization of the Helmholtz equation. For brevity, the FEM formulation of Helmholtz equation is not presented here. Starting from the FEM matrix system of Helmholtz equation,

$$[M]\{U_i\} = \{F\} \tag{22}$$

Next, we integrate the boundary unknowns into the FEM matrix system, we have

$$\begin{bmatrix} M_i & 0 \\ 0 & M_b \end{bmatrix} \begin{Bmatrix} U_i \\ U_b \end{Bmatrix} = \begin{Bmatrix} F_i \\ F_b \end{Bmatrix} \tag{23}$$

where the boundary operator matrix M_b subject to two sets of equations with respect to the two complementary operators,

$$M_{kj}^{b} u_j = f_k^{b}, M_{kj}^{\bar{b}} \bar{u}_j = f_k^{b} \tag{24}$$

The next step is to average the C-COM zone solutions of the two sets of complementary operations. Right on the interface perimeter of C-COM zone and interior computational domain, the nodal fields subject to two sets of equations

$$M_{k,j-1} u_{j-1} + M_{k,j} u_j + M_{k,k-1} u_{k-1} + M_{k,k} u_k + M_{k,k+1} u_{k+1} + M_{k,m} u_m + M_{k,m+1} u_{m+1} = 0 \tag{25}$$

$$M_{k,j-1} \bar{u}_{j-1} + M_{k,j} u_j + M_{k,k-1} \bar{u}_{k-1} + M_{k,k} u_k + M_{k,k+1} u_{k+1} + M_{k,m} u_m + M_{k,m+1} u_{m+1} = 0 \tag{26}$$

$$let \;\; u_{j-1} = \frac{(\bar{u}_{j-1} + u_{j-1})}{2}, u_{k-1} = \frac{(\bar{u}_{k-1} + u_{k-1})}{2},$$

$$\begin{aligned} &M_{k,j-1}(\bar{u}_{j-1} + u_{j-1})/2 + M_{k,j} u_j + M_{k,k-1}(\bar{u}_{k-1} + u_{k-1})/2 + M_{k,k} u_k \\ &+ M_{k,k+1} u_{k+1} + M_{k,m} u_m + M_{k,m+1} u_{m+1} = 0 \end{aligned} \tag{27}$$

The C-COM can then be implemented easily by modifying the coefficients matrix in the FEM matrix system. The averaging layer in a FEM system, using triangle elements, is illustrated in Fig. 20.

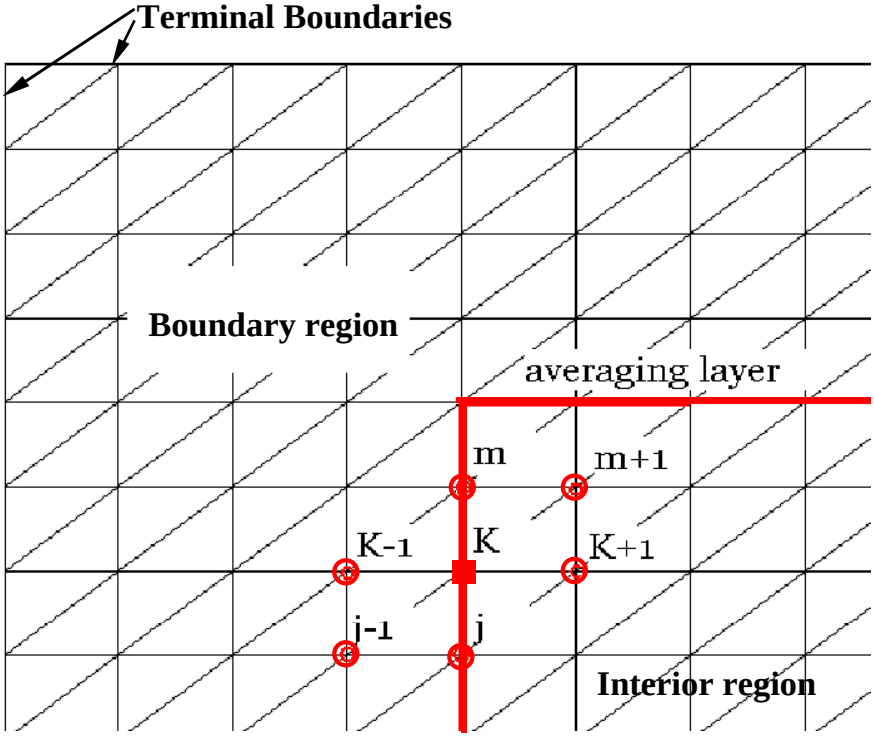

Fig. 20. FEM C-COM implementation illustration.

To test the absorption effectiveness of the C-COM in FEM, we consider a two-dimensional radiation problem with a current excitation located right at the center of the computational domain. The computational domain is $20\Delta \times 20\Delta$, (In numerical experiments given here, the grid will be uniform in the x- and y-directions with $\Delta = 0.025\lambda$.).

Let the exact field at each of the monitor points be E^{ex}. The normalized percentage error is then given by

$$Normalized\ Error = 20\log_{10}\left|\frac{E^{ex} - E^{c-com}}{E^{ex}}\right| \qquad (28)$$

The exact solution, E^{ex} is obtained from the series solution. The normalized error of the numerical experiments using C-COM4 is shown in Fig. 21. The maximum reflection observed is –45 dB, which occurs at the neighbor nodes of the source.

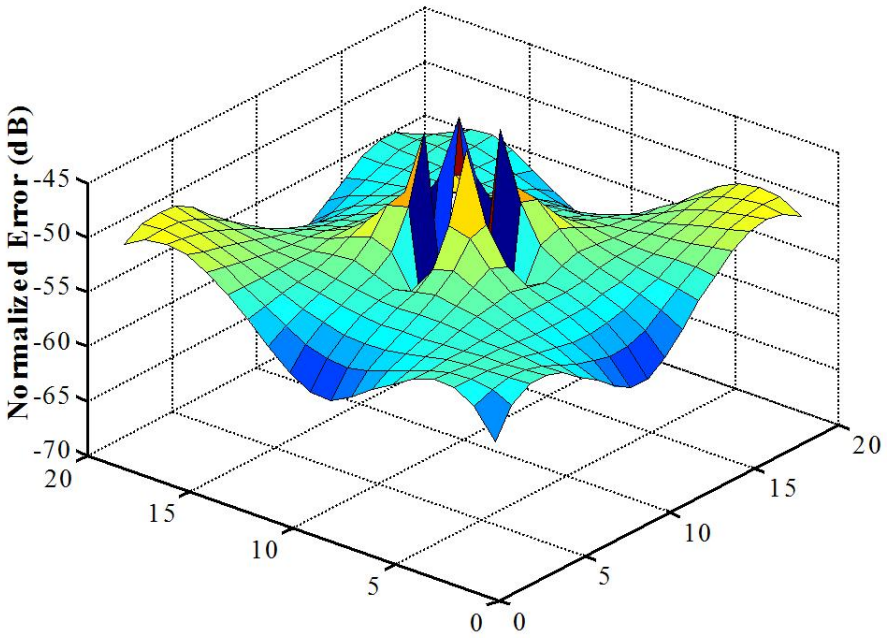

Fig. 21. The normalized error of the numerical experiment using C-COM4 in FEM.

B. Comparison Study of C-COM and PML in Finite Element Method

A comparison study between C-COM and PML is conducted on a two-dimensional parallel plate waveguide. The waveguide is excited with a TEM mode. The waveguide is sketched as Fig. 22.

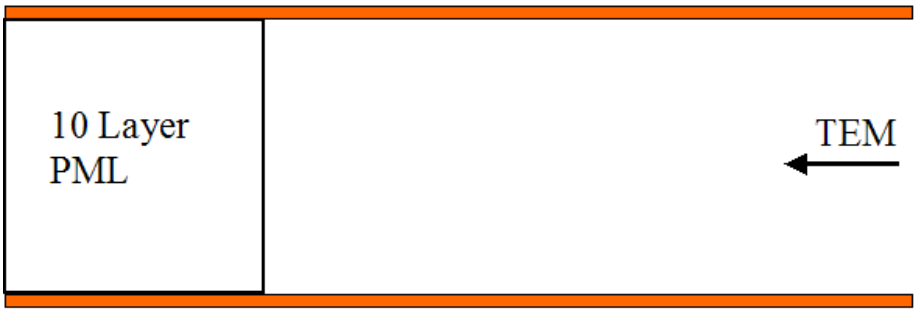

Fig. 22. Waveguide terminated with a 10-layer PML.

For the PML terminated waveguide, a ten-layer PML medium was used. Three different discretizations (mesh#1=2698 nodes, mesh#2=5831 nodes, mesh#3=11514 nodes) were considered [33]. The corresponding reflection coefficient observed at a fixed distance from the PML layers (0mm in this case) as a function of frequency for TEM is shown in Fig. 23. It was shown that the lowest reflection at the observed point of the reported PML termination is about –90 dB. Since PML consists of lossy material layers to absorb outgoing wave, thus the reflection is both frequency dependent and mesh density (grid size) dependent.

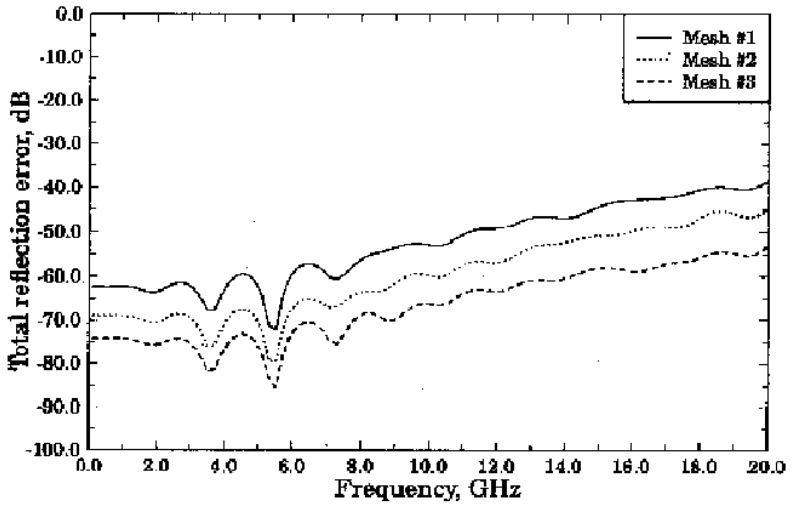

Fig. 23. Normalized reflection error due to PML termination for various number of finite elements, TEM mode, 10 layer PML [33].

When a TEM is excited in a waveguide terminated with C-COM4, the reflection is independent of the frequency. This is because of the finite difference scheme nature of the way C-COM applied in frequency domain, which is integrated in the FEM matrix system. To obtain the accuracy, the spatial step used in the finite difference scheme is required to be less than $1/10^{th}$ of the wavelength. In our numerical experiments, the spatial step is normalized to wavelength. However, the reflection is space dependent. The corresponding error of the waveguide for C-COM2, which means C-COM applied to a second BT boundary condition, C-COM2, C-COM3, and C-COM4 are illustrated in Fig. 24 (a), (b), and (c) respectively. The observed reflections indicate that with a C-COM4 boundary condition, we can reach an extremely low reflection up to –130 dB without increasing the computational resource consumption when comparing with PML.

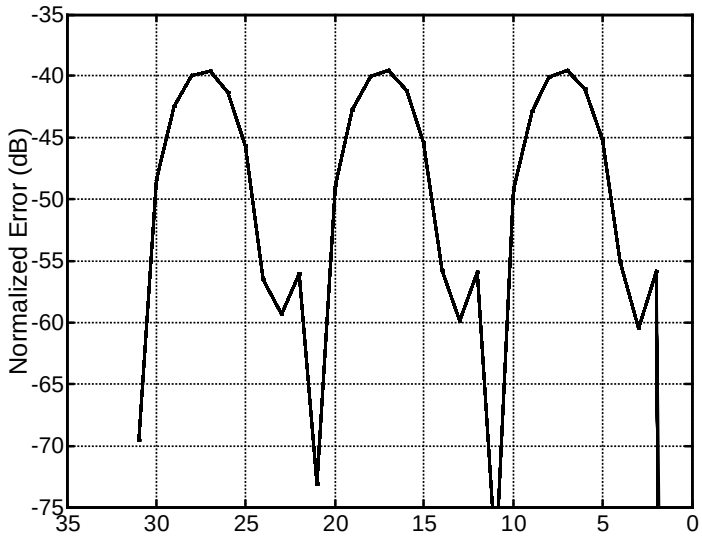

(a)

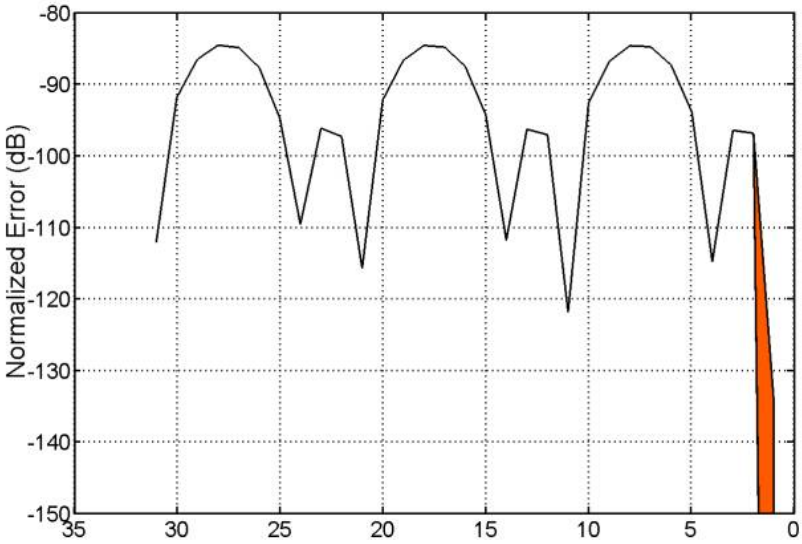

(b)

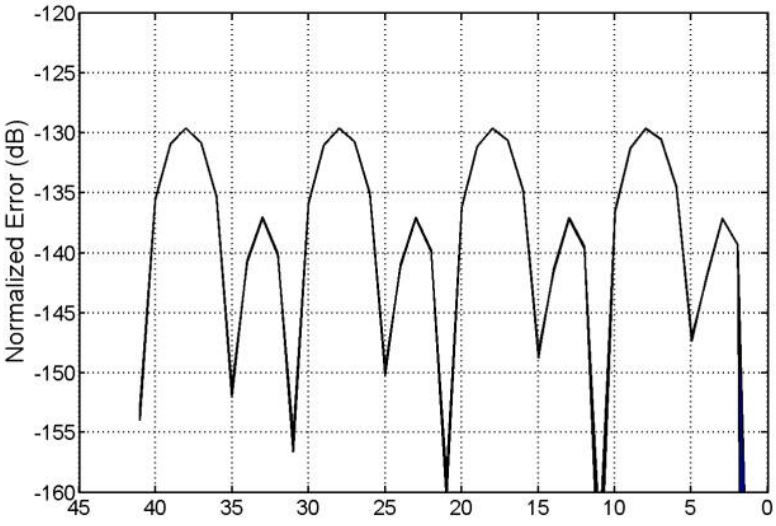

(c)

Fig. 24. Normalized Error of C-COM in FEM, for TEM mode in a parallel plate waveguide, (a). C-COM2, (b). C-COM3, (c). C-COM4.

III.4 CONCLUSIONS

In this chapter, the applications of C-COM in open-region simulations are presented to demonstrate the high accuracy of C-COM. The simulations using C-COM as a boundary mesh truncation technique here include the C-COM for Liao's ABC in FDTD, the C-COM for Bayliss-Turkel ABC in both Finite Difference Frequency-Domain and Finite Element Method. Free space current source radiation, two-dimensional scattering problems and guided wave propagation problems are investigated. These simulations showed that with C-COM, the reflection arising from the original ABCs can be significantly reduced in both time-domain and frequency-domain simulations. The comparison between PML and C-COM in time-domain and frequency-domain simulations also demonstrated that the C-COM is a highly efficient and highly accurate mesh truncation technique.

IV. STABILITY ANALYSIS OF OPEN-REGION FINITE DIFFERENCE TIME-DOMAIN SIMULATION

In an open-region electromagnetic FDTD simulation, the Yee scheme is used to discretize Maxwell's curl equations in the interior computational domain [34]-[35]. On the outer boundary, an absorbing boundary condition (ABC) or mesh truncation technique is applied and then implemented using *a specific* finite difference scheme. The implementation of the boundary condition strongly affects the accuracy of the overall simulation as has been documented extensively in numerous publications [6]-[15]. However, what has received much less attention is the effect of the discrete form of the analytic boundary conditions, or more precisely its implementation, on the stability of the solution. This work aims to, first, address critical issues related to the instability generated by boundary conditions, and second, to introduce an analysis method that is consistent with numerical experiments.

In the electromagnetic computational context, instability is generally referred to the time-dependent growth of the solution such that it violates the physical phenomenon being simulated. When boundary conditions (or mesh-truncation techniques) are applied at the boundary of the computational domain, instability of the overall solution can occur. Different methods have been applied to study the stability behavior induced by the boundary conditions. In [22]-[24], the GKS (Gustafsson, Kreiss, and Sundström) theory, referred as Z-transform analysis, was used to investigate the stability of Higdon's and Liao's absorbing boundary conditions. Higdon discussed the stability of the Higdon's ABC by using the Kreiss theorem and GKS theory [25]. Wang and Tripp applied the von

Neumann analysis to Liao's ABC [26]. From these previous works, the boundary scheme induced instability was, in certain cases, eliminated by enforcing the so-called stabilizing or damping factors in the difference schemes. However, while these previous works predict that the instability is ensured once stabilizing or damping factors are introduced, numerous numerical simulations conducted by these authors revealed that instability was strongly evident in the solution despite the introduction of damping factors.

In [27], Ramahi, through empirical experiments, found, that the Cartesian-based computational domain results in certain numerical irregularities, particularly in the corner regions of the domain. More specifically, Ramahi found that the stencil used to describe (discretize) the boundary condition leads to numerical crosstalk. These irregularities act as a source of catastrophic instability (i.e., instability that grows very large in a relatively small number of time steps) [27]. The computational geometry could introduce the corner instability arising from the crosstalk between fields of the internal grids and the fields on the boundary. Although the cause of the corner instability is identified, it is suspected that this source of instability can be mitigated by introducing a quarter-pi shape corner region that will inherently eliminate the possibility of stencil cross talk amongst boundary nodes [27]. The quarter-pi corner region, however, can introduce interpolation errors that can prove equally detrimental to the overall accuracy of the simulation.

While the work in [36] uncovered a critical mechanism that produces instability in FDTD simulation, it did not isolate a small, yet important growth in the solution that can easily be overshadowed by more pronounced growth generated by the instability arising from the corner regions [37]. It is these observations that created the impetus behind this present work.

In this work, we refer to the finite difference scheme used to convert Maxwell's equations into a discrete form in the internal computational region as the *internal scheme*. Similarly, we refer to the finite difference scheme used to discretize the boundary conditions as the *boundary scheme*. In section IV.1, we briefly review the instability criteria for the internal and boundary schemes. We show that numerous previous works established that the stability behavior of the FDTD solution depends not only on the internal scheme, but also on the boundary scheme. By applying the von Neumann analysis on the Higdon's ABC, we show that for a linear, constant coefficient, one-time step (first-order time derivative) difference scheme, the stability analyses obtained using different methods, such as GKS and Kreiss theories, yield identical results to those obtained using the von Neumann analysis. In section IV.2, we present empirical findings that conclusively prove that satisfying the stability requirements of the internal scheme and boundary scheme is not sufficient to guarantee the stability of FDTD simulation. In section IV.3, we introduce a method based on the discrete-time system stability analysis to predict the instability induced by the coupling between internal grids and boundary nodes. We refer to this method as Coupled Stability Analysis. The new stability analysis is applied to Higdon's second and third-order absorbing operators.

IV.1 STABILITY OF INTERNAL SCHEME AND BOUNDARY SCHEME

IV.1.1 Stability of Yee Scheme

In the classical FDTD method, the Yee scheme is used to discretize Maxwell's curl equations in the interior of the computational domain (for details, please refer to appendix A.1). For brevity we will not state the full description of the FDTD discrete set of equations corresponding to (1); the reader is referred to [6] and references therein for an exhaustive discussion of the FDTD method.

The stability requirement of the Yee scheme is given by applying the Courant-Friedrichs-Lewy (CFL) condition. The CFL condition identified a fundamental and necessary condition for convergence of any numerical approximation of a partial differential equation, linear or non-linear. For linear problems, the convergence is equivalent to stability. This equivalence leads to the CFL condition for stability. The weakness of the CFL condition is that it is necessary but not sufficient for convergence. For two-dimensional problems, the stability criterion of the Yee scheme, referred as the Courant limit in FDTD, is given as

$$\Delta t \le \Delta t_c = \frac{1}{c\sqrt{\frac{1}{(\Delta x)^2}+\frac{1}{(\Delta y)^2}}}, \qquad (1)$$

where Δt is the time increment; Δx, Δy are the space increment in x direction and y direction, respectively, and c is the speed of light.

IV.1.2 Stability of Boundary Scheme

The stability analysis methods applied on the boundary scheme include the von Neumann condition, Kreiss and GKS (Gustafsson, Kreiss, and Sundström) theories. These methods are all based on the Fourier transform representation of the solution. For one-step, linear, constant coefficient finite-difference formulae on regular grids of partial differential equation, the von Neumann condition gives a necessary and sufficient stability criterion. The Kreiss theory asserts that a "first-order linear hyperbolic system with a left-hand boundary condition is stable if and only if it admits no solutions without any left reflection". The GKS theory is a discrete analogue of the Kreiss theorem, which is developed for continuous problem [38]-[41].

Stability analyses were applied to two popular absorbing boundary operators: the Liao's and Higdon's ABCs. The investigation of the stability induced by applying Liao's ABC can be found in [22], [23], [26]. It was found that when the frequency approaches zero, the Liao's boundary operator approaches zero, leading to instability. A damping factor was proposed to stabilize the boundary scheme. The stability analysis results in [22], [23] are identical to the conclusion in [26], in which the von Neumann condition was used to study the stability of Liao's ABC.

When Higdon's boundary operators were used, it was found that there is a breakdown in the Kreiss theory at zero frequency; consequently, it was conjectured that the instability was related to the harmonics close or equal to DC [25]. In [41], it was argued that the instability was possibly triggered by an incompatibility between the initial data and the boundary conditions. The zero frequency instability was reported in [43] as

well. A constant, which we referred as damping or stabilizing factor, was introduced as the frequency approaches zero to prevent the boundary operator from becoming zero.

Higdon's absorbing boundary condition is based on the one-way wave equation. The N^{th} order Higdon ABC is given by

$$\prod_{i=1}^{N}(\partial_x + \frac{\cos\phi_i}{c}\partial_t + \alpha_i)U = 0, \tag{2}$$

where c is the light speed, ϕ_i is the incident angle for which the boundary condition is perfectly absorptive, and α_i is a damping factor [41]. To discretize (2) into a finite difference equations, we use the following operators

$$\partial_x \to \left(\frac{I - S^{-1}}{\Delta x}\right)\left((1-a)I + aT^{-1}\right) \tag{3}$$

$$\partial_t \to \left(\frac{I - T^{-1}}{\Delta t}\right)\left((1-b)I + bS^{-1}\right), \tag{4}$$

where I is the identity operator, S^{-1} is the space-shift operator, and T^{-1} is the time-shift operator. The choice of the weighting coefficients a and b give different difference scheme including the forward Euler ($a=0$, $b=1$), backward Euler ($a=b=0$), box scheme ($a=b=0.5$), … etc. In general, the weighting coefficients are positive real numbers bounded by unity. The shift operators are explicitly expressed as:

$$\begin{aligned}
&IU(t=n, x=x_a, y=y_b) = U(t=n, x=m\Delta x, y=l\Delta y) = u_{m,l}^{n} \\
&T^{-i}U(t=n, x=x_a, y=y_b) = U(t=n-i\Delta t, x=m\Delta x, y=l\Delta y) = u_{m,l}^{n-1} \\
&S_x^{-i}U(t=n, x=x_a, y=y_b) = U(t=n, x=m\Delta x - i\Delta x, y=l\Delta y) = u_{m-i,l}^{n} \\
&S_y^{-i}U(t=n, x=x_a, y=y_b) = U(t=n, x=m\Delta x, y=l\Delta y - i\Delta y) = u_{m,l-i}^{n} \\
&i = 1,2,3...N
\end{aligned} \tag{5}$$

Consider a computational domain bounded on the right-hand-side by $x=x_{a,}$ where $x_a \geq x \geq 0$. Substituting the operators (3) and (4) into (2), we have

$$B_N U = \prod_{i=1}^{N} (I + a_i T^{-1} + b_i S^{-1} + c_i S^{-1} T^{-1}) U = 0, \tag{6}$$

where

$$\begin{aligned} a_i &= \frac{-(a - h(1-b))}{a - 1 - h(1-b) - \alpha_i \Delta x} \\ b_i &= \frac{-(a - 1 + hb)}{a - 1 - h(1-b) - \alpha_i \Delta x} \\ c_i &= \frac{-(-a - hb)}{a - 1 - h(1-b) - \alpha_i \Delta x} \\ h &= \frac{\cos \phi_i}{c} \frac{\Delta x}{\Delta t} \end{aligned} \tag{7}$$

From (6), the difference formula of the first-order Higdon's ABC (i.e., $N=1$), is a one-time step, linear, constant coefficient scheme. Furthermore, the difference scheme of the higher-order Higdon ABC (i.e., $N \geq 2$) is also a linear and constant coefficient formula since it is derived by cascading first-order formula.

The von Neumann analysis is based on the Fourier representation of the explicit solution. In our problem, we replace the field at the node (n,m), $u(n,m)$, with a Fourier representation of the solution, $u(n,m)=g^n e^{jm\theta}$, where $\theta=k_x \Delta_x$, $\theta \in [-\pi, \pi]$ [40]. A stable solution requires that the magnitude of any time-harmonic component (Fourier component) to remain bounded in time. Substituting $u(n,m)=g^n e^{jm\theta}$ into (6), we obtain the amplification factor

$$g_i = \frac{-a_i e^{j\theta} - c_i}{e^{j\theta} + b_i}, \; i = 1,2,3..., N \tag{8}$$

For the second or higher order Higdon's ABC *(N≥2)*, the amplification factor is a *multiple* root.

The stability of the boundary scheme requires that the amplification factor satisfies $|g_i(\theta)|< 1$, $\theta\in[-\pi,\pi]$ for the second or higher order Higdon's ABC. From equation (8), the magnitude of the amplification factor depends on h and $\alpha_i\Delta x$. The coefficient, h, is set by the stability requirement of the internal scheme (satisfying the Courant limit). The damping factor, α_i, is crucial to the stability of the boundary scheme. For $\alpha_i=0$, and $a=b$, $|g_i(\theta)| =1$ at $\theta=0$, as shown in Fig. 25. Since for the second or higher-order Higdon's ABC, the root is a *multiple* root, the scheme is unstable. When $a\neq b$, the same behavior is observed, i.e., at $\theta=0$, $|g_i(\theta)| =1$, as can be seen in Fig. 26. Therefore, based on the von Neumann analysis, the second or higher order Higdon's ABCs are unstable for $\alpha_i=0$. (Notice that for $\theta=0$, the Fourier representation of the solution corresponds to the zero frequency, which is consistent with the observation in [25], [43], [43].)

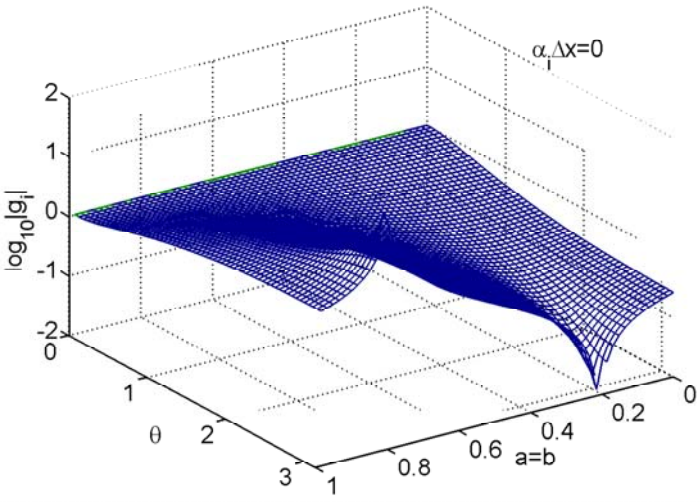

(a)

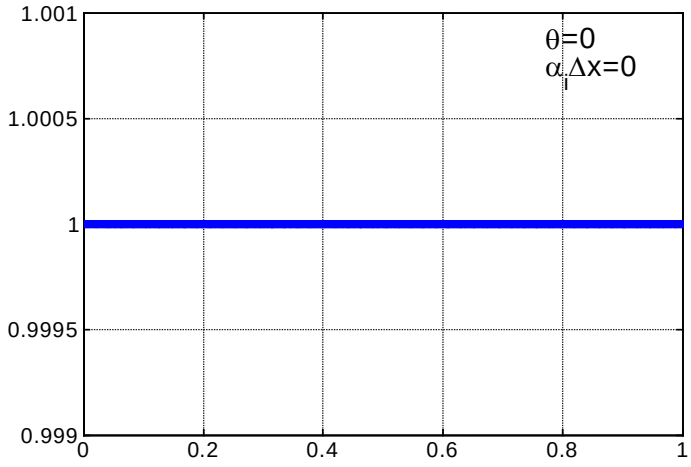

(b)

Fig. 25. Magnitude of the amplification factor at $a=b$, $\alpha_i\Delta x=0$. (a). $\theta=[0, \pi]$ (b). $\theta=0$.

Next, we consider the effect of introducing a small damping factor term, $\alpha_i\Delta x=\varepsilon$, $0<\varepsilon<<1$. Higdon originally introduced α_i to mitigate instability [41]. Previous work has

shown that α_i has to be small enough in order not to affect the low-frequency behavior of the solution [24].

Let us consider the case for $\alpha_i \Delta x$=0.0001, and a=b. Because of symmetry, it is sufficient to consider $\theta \in [0,\pi]$. Fig. 27 (a) and (b) show the amplification factor to be less than unity, thus implying that the boundary scheme can be made stable by the addition of a small loss factor, α_i.

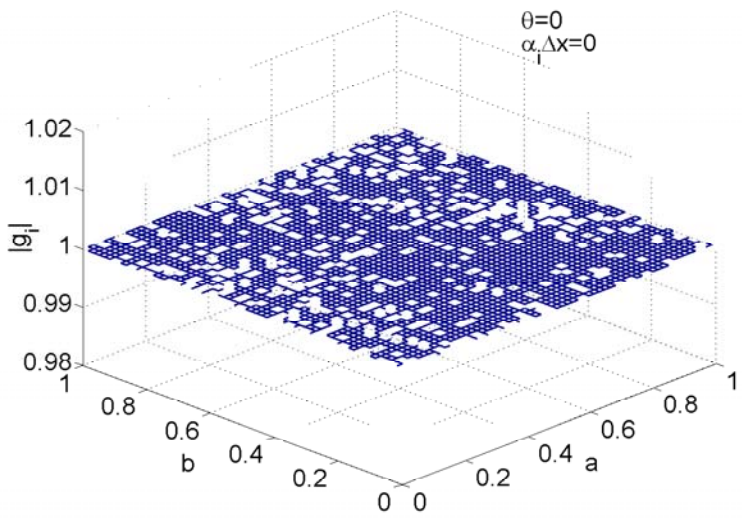

Fig. 26. Magnitude of the amplification factor at $a \neq b$, $\theta=0, \alpha_i \Delta x=0$. (The graph is generated by Matlab®. Note that the voids of the graph are due to display effects.)

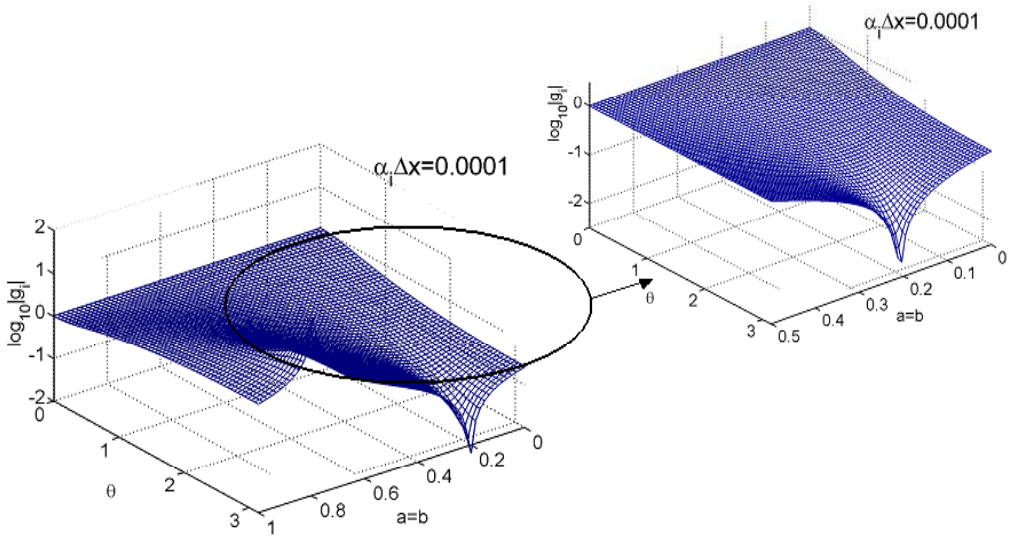

(a)

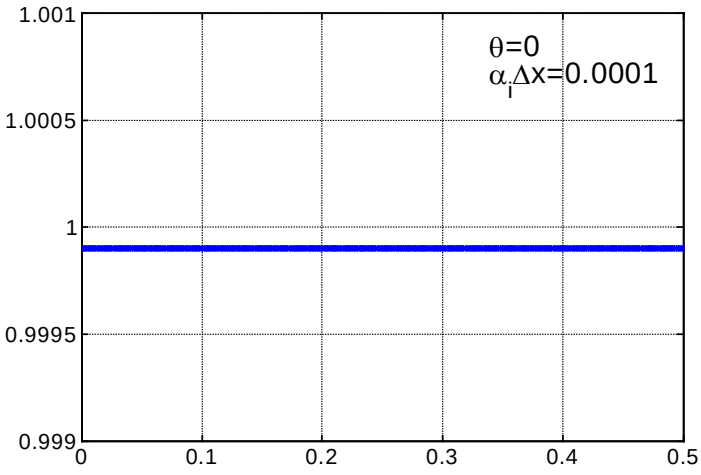

(b)

Fig. 27. Magnitude of the amplification factor at $a=b$, $\alpha_i\Delta x$=0.0001 (a) $a=b=[0,1]$ (b) $\theta=0$, $a=b=[0,0.5]$.

When $a\neq b$, we consider the behavior of $|g_i(\theta)|$at $\theta=0,\pi$ first and then examine the general case $0<\theta<\pi$. For the case $\theta=0,\ \pi$, $g_i(\theta)$ remains bounded as clearly seen in Fig.

28 (a) and (b). For $0<\theta<\pi$, by using multivariable optimization in Matlab, we find that for a small damping factor of $\alpha_i\Delta x=0.0001$, $g_i(\theta)$ remains bounded by unity for $a\leq 0.5$, $b\leq 0.5$. Furthermore, as $\alpha_i\Delta x$ increases $|g_i(\theta)|$ decreases, however, this adversely affects the lower frequencies behavior of solution.

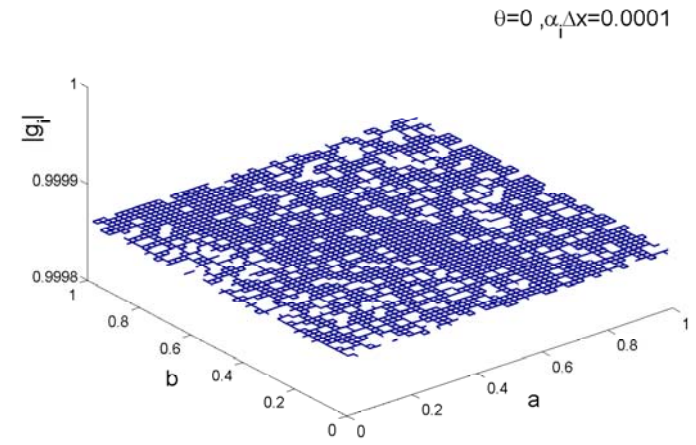

(a)

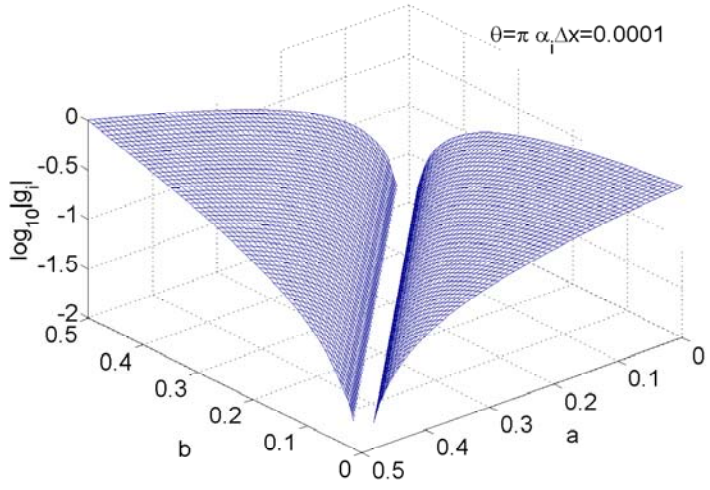

(b)

Fig. 28. Magnitude of the amplification factor at $\alpha_i\Delta x$=0.0001, $a\neq b$, (a)$\theta=0$, (b)$\theta=\pi$.

As a conclusion, the von Neumann analysis when applied on the boundary schemes predicts that the numerical solution will be stable providing that $a \le 0.5$, $b \le 0.5$, and the factor α_i, satisfies that $\alpha_i \Delta x > 0$. These results are identical to those predicted in [24]-[25], [41]-[43], where the GKS condition was used. Therefore, as a summary, the von Neumann and GKS analyses yield the following conditions for stability:

$$\begin{aligned} &\Delta t \le \frac{1}{c\sqrt{\frac{1}{(\Delta x)^2}+\frac{1}{(\Delta y)^2}}} \\ &0 < \alpha_i \Delta x \\ &a \le 0.5, b \le 0.5 \end{aligned} \tag{9}$$

IV.2 MILD AND CATASTROPHIC INSTABILITY

In section II it was shown that Higdon's ABCs of *any order* can be stabilized by the introduction of a small loss factor, α_i. However, several researchers including the authors of this work have repeatedly observed numerical instability even when the internal stability criterion is satisfied and a non-zero loss factor, α_i, is added. In this section, we show several numerical examples that give rise to different forms of instability not predicted by previous analyses. Depending on the speed by which the solution "blows up", we classify the instabilities as either *mild* or *catastrophic*. Before going any further, one might question the practicality of looking into the stability behavior after the elapse of thousands or even hundreds of thousands of time steps. In many practical scenarios in electromagnetic simulations, especially in the analysis of

resonant structures, the energy lingers within the system for long period of time and dissipates very slowly. To capture the low frequency behavior of the response of such resonant systems, which typically corresponds to the slow dissipation of energy, large number of time steps is essential, and it is not uncommon to run simulations for hundreds of thousands of time steps. (For a sample of the type of practical problems encountered in electromagnetic applications, the reader is referred to [44].

In [27], it was observed by Ramahi, that the corner region in the FDTD computational domain is a source of the catastrophic instability. This finding is demonstrated by a simple experiment in which a line source is placed in the center of a computational domain of size 40 Δx x 50 Δy. The domain is then elongated to 40Δx x 500Δy, 40Δx x 2000Δy, 40Δx x 4000Δy, and 40Δx x 8000Δy, while the instant at which the instability occurs is observed. Fig. 29 shows the electric field at an observation point that is fixed with respect to the location of the source. (The observation point is offset by (+3Δx, +4Δy).)

Simple observation shows that the dramatic (artificial) increase in the solution occurs precisely at the location of the corner. Further discussion on this experiment can be found in [27]. It was concluded in [27], that the only source of instability arises from the corner region of the computational domain. However, this conclusion, even though supported by previous works and empirical findings, overlooked a mild form of instability.

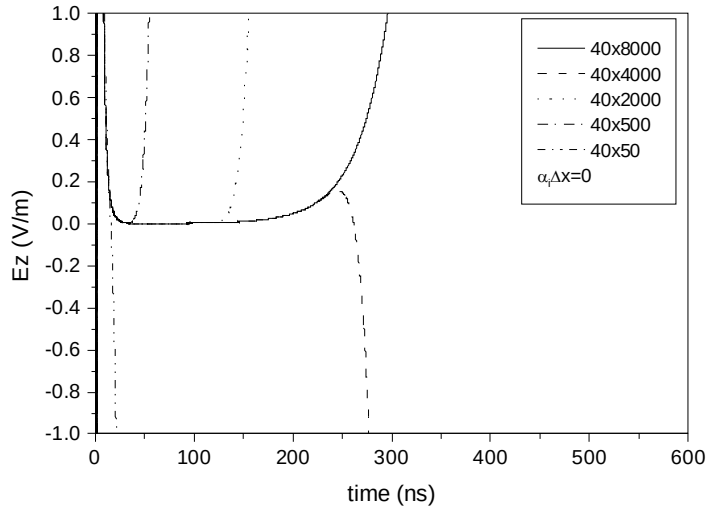

Fig. 29. Observed instability when using Higdon's fourth-order ABC with no damping.

In accordance with the conclusion reached in section II above, if a damping factor is inserted in Higdon's ABC and the weighting functions *a* and *b* were made to satisfy the conditions $a \leq 0.5$, $b \leq 0.5$, then the boundary scheme should be stable. Applying a small loss factor $\alpha_i \Delta x = 0.0001$, and adhering to the stability criterion, we repeat the above experiment and observe in Fig. 30 a *mild* form of instability that precedes the instability that arise from the corner region. The same experiment is repeated with Higdon's third-order ABC, and similar results are observed. Fig. 31 and Fig. 32 show that the instability arising from the corner regions proceeds the instability arising from the boundary. These two experiments conclusively demonstrate that the boundary itself and the corner regions, both contribute uniquely to instability.

The important conclusion that is reached here is the following: When using the FDTD method to solve open-region radiation problems, the numerical solution can

experience instability even though the Courant limit and the boundary stability criterion (9) are both satisfied. These findings lead to an investigation of an alternative analysis that can provide consistent prediction of instability. This analysis will be referred to as Coupled Stability Analysis.

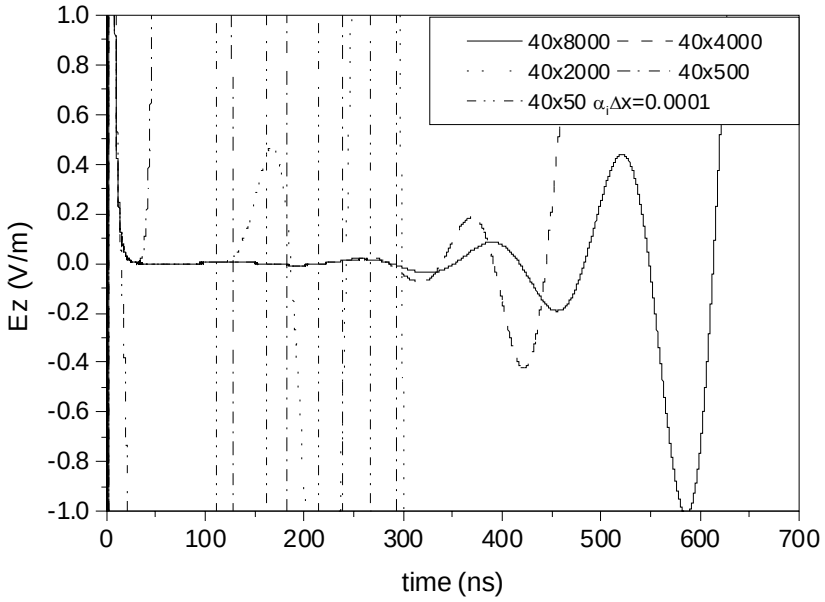

Fig. 30. Observed instability when using Higdon's fourth-order ABC with a damping factor.

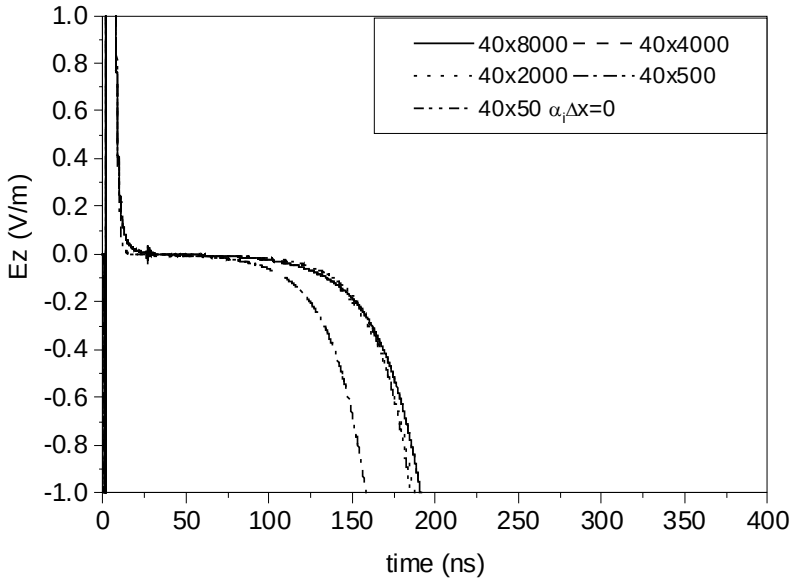

Fig. 31. Observed instability when using Higdon's third-order ABC with no damping.

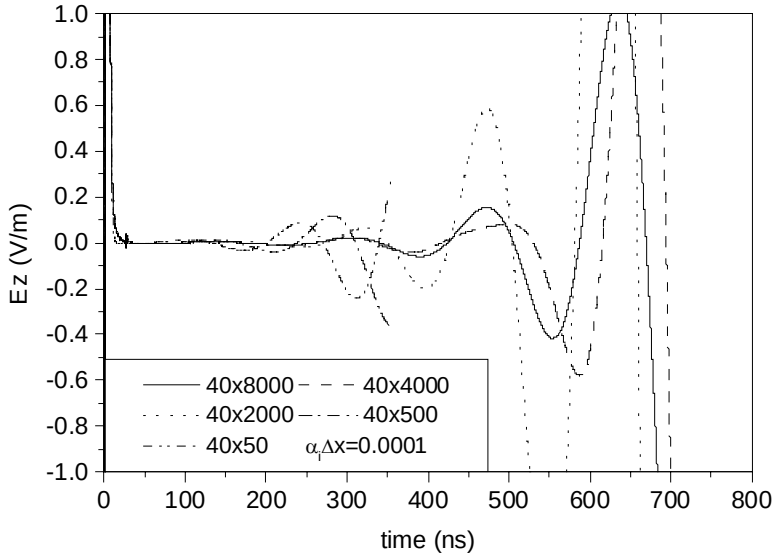

Fig. 32. Observed instability when using Higdon's third-order ABC with a damping factor.

IV.3 COUPLED STABILITY ANALYSIS

IV.3.1 Theory

Since no boundary condition can work perfectly to absorb all waves incident at the boundary, some energy reflects back into the computational domain. This very reflection causes the interference between the fields solved for by the internal scheme and the fields generated by the boundary scheme. To characterize any potential instability due to this interference, it is natural to expect that neither the internal scheme nor the boundary scheme can be considered separately. In this section, an analysis method is introduced that couples the interior solution to the boundary fields based on the stability analysis of a linear time-invariant (LTI) discrete system.

A. Stability of linear time-invariant discrete system

In discrete signal processing theory, the system function is defined as the Z-transform of the output series divided by the Z-transform of the input series. A linear time-invariant (LTI) discrete system is asymptotically stable if the output series resulting from the initial energy decays to zero as the discrete time index becomes large. The system is marginally stable if the magnitude of output series is less than some finite positive constant [45], [46].

Consider the linear time-invariant finite dimensional discrete-time system given by the system transfer function *H(z)*:

$$H(z) = \frac{N(z)}{(z - p_1)(z - p_2)\cdots(z - p_n)} \tag{10}$$

where $p_1, p_2,\ldots, p_n$ denote the poles of $H(z)$, and $N(z)$ is a polynomial. The system $H(z)$ is asymptotically stable *if and only if*

$$| p_i | < 1 \quad \text{for } i=1,2,\ldots,n \tag{11}$$

Based on the LTI theory, the system is marginally stable if and only if $| p_i | \leq 1$ for all non-repeated poles, and $| p_i | < 1$ for all repeated poles. In the complex plane, if we define the closed unit-disc to be the open unit-disc plus the unit circle, then the system is unstable if there are one or more poles outside the closed unit-disc, or if there are repeated poles on the unit-circle.

B. LTI discrete system defined by boundary difference schemes

In the FDTD method, the space and time are discretized and the fields are sampled in both time and spatial domains. At each node in the computational domain, the fields solved by using the FDTD method results in a discrete series with sampling frequency $f_s=1/\Delta t$. In this discrete time series, the nth number in the sequence is $u[n] = u(n\Delta t)$.

When an absorbing boundary condition is applied to truncate the computational domain, the interior fields and the boundary fields are related through the difference scheme of the absorbing boundary condition. As the sampled interior fields and boundary fields are both discrete series, the relationship defined by the difference scheme of ABC will be considered here as defining the *discrete system*. In this system, the boundary fields are treated as output while the interior fields are treated as inputs.

The difference scheme of ABC, whether they are derived numerically or analytically, is a linear combination of the discrete sequences of the interior nodes and

the interior nodes at previous time steps. Therefore, the system defined by the boundary difference scheme is also a linear system. This system is causal because the output, which is the boundary fields sequence, is dependent only on the present and past values of the inputs. From the linearity property of the system, it can also be proved that this system is time-invariant, which means that a time shift in the input sequence causes a corresponding time shift in the output sequence. As a result, we conclude that the system defined by the difference scheme of ABCs is a LTI discrete system.

C. Coupled stability analysis

Let us consider a boundary normal to the *x*-axis. Denoting the Z-transform operation by $\mathcal{Z}$, we apply the Z-transform on the boundary field designated by the spatial index *m* (corresponding to discretization along the *x* axis) and temporal index *n*, we have

$$Y(z) \equiv \mathcal{Z}(u_m^n) \tag{12}$$

Next, we apply the Z-transform on the fields at the boundary, but at previous time steps; from the Z-transform properties, we have:

$$\begin{aligned} &\mathcal{Z}(u_m^{n-1}) = z^{-1}Y(z) \\ &\mathcal{Z}(u_m^{n-2}) = z^{-2}Y(z) \\ &\ldots \\ &\mathcal{Z}(u_m^{n-L}) = z^{-L}Y(z) \end{aligned} \tag{13}$$

Applying Z-transform on the internal fields for the time step *n*, we have:

$$\begin{aligned} &X_1(z) = \mathcal{Z}(u_{m-1}^n) \\ &X_2(z) = \mathcal{Z}(u_{m-2}^n) \\ &\ldots \\ &X_N(z) = \mathcal{Z}(u_{m-N}^n) \end{aligned} \tag{14}$$

Note that L and N depend on the length of the numerical stencil of the boundary condition in space and time respectively.

Since the fields are subject to the wave equation, and since the boundary condition is not perfectly absorbing, we must assume the presence of a two-way propagating wave traveling along the x direction at each spatial node. We have

$$\begin{aligned}
u_m^n &= (e^{jn\omega\Delta t - jmk_x\Delta x} + R_d\ e^{jn\omega\Delta t + jmk_x\Delta x})e^{-jlk_y\Delta y} \\
u_{m-1}^n &= (e^{jn\omega\Delta t - j(m-1)k_x\Delta x} + R_d\ e^{jn\omega\Delta t + j(m-1)k_x\Delta x})e^{-jlk_y\Delta y} \\
u_{m-2}^n &= (e^{jn\omega\Delta t - j(m-2)k_x\Delta x} + R_d\ e^{jn\omega\Delta t + j(m-2)k_x\Delta x})e^{-jlk_y\Delta y} \\
&\cdots \\
u_{m-N}^n &= (e^{jn\omega\Delta t - j(m-N)k_x\Delta x} + R_d\ e^{jn\omega\Delta t + j(m-N)k_x\Delta x})e^{-jlk_y\Delta y},
\end{aligned} \tag{15}$$

where k_x is the wave number in the x direction, k_y is the wave number in the y direction and R_d is the reflection coefficient. In the discrete domain, the reflection coefficient R_d is a function of Δx and Δt but independent of the sequence number n. Since we are interested in the behavior of the fields at a boundary normal to the x-axis, the y-dependence in (15) is ignored.

The Z-transforms of the discrete series described in (15) are

$$\begin{aligned}
Y(z) &= \mathcal{Z}(u_m^n) = e^{-jlk_y\Delta y}\mathcal{Z}(e^{jn\omega\Delta t - jmk_x\Delta x} + R_d\ e^{jn\omega\Delta t + jmk_x\Delta x}) \\
X_1(z) &= \mathcal{Z}(u_{m-1}^n) = e^{-jlk_y\Delta y}\mathcal{Z}(e^{jn\omega\Delta t - j(m-1)k_x\Delta x} + R_d\ e^{jn\omega\Delta t + j(m-1)k_x\Delta x}) \\
X_2(z) &= \mathcal{Z}(u_{m-2}^n) = e^{-jlk_y\Delta y}\mathcal{Z}(e^{jn\omega\Delta t - j(m-2)k_x\Delta x} + R_d\ e^{jn\omega\Delta t + j(m-2)k_x\Delta x}) \\
&\cdots \\
X_N(z) &= \mathcal{Z}(u_{m-N}^n) = e^{-jlk_y\Delta y}\mathcal{Z}(e^{jn\omega\Delta t - j(m-N)k_x\Delta x} + R_d\ e^{jn\omega\Delta t + j(m-N)k_x\Delta x})
\end{aligned} \tag{16}$$

Using the linearity property of the Z-transform, and equations (14) to (16), the Z-transform of the internal series $\{X_2(z), X_3(z), \ldots, X_N(z)\}$, can be denoted as a linear combination of $X_1(z)$, and $Y(z)$. To show this, we consider, as an example, a second-order

absorbing boundary condition. The boundary field u_m^n is calculated from the grid fields u_{m-1}^n, u_{m-2}^n. Since the reflection R is independent of the sequence number n, hence, applying the Z-transform on the grid fields $u_m^n, u_{m-1}^n, u_{m-2}^n$, we have

$$\begin{aligned} Y(z) &= \mathcal{Z}(u_m^n) = e^{-jlk_y\Delta y}(e^{-jmk_x\Delta x} + R_d\ e^{jmk_x\Delta x})\mathcal{Z}(e^{jn\omega\Delta t}) \\ X_1(z) &= \mathcal{Z}(u_{m-1}^n) = e^{-jlk_y\Delta y}(e^{-j(m-1)k_x\Delta x} + R_d\ e^{j(m-1)k_x\Delta x})\mathcal{Z}(e^{jn\omega\Delta t}) \\ X_2(z) &= \mathcal{Z}(u_{m-2}^n) = e^{-jlk_y\Delta y}(e^{-j(m-2)k_x\Delta x} + R_d\ e^{j(m-2)k_x\Delta x})\mathcal{Z}(e^{jn\omega\Delta t}) \end{aligned} \tag{17}$$

After simple algebraic manipulation of the equations in (17), the relationship between $X_2(z)$, $X_1(z)$, and $Y(z)$ is derived:

$$X_2(z) = 2\cos(k_x\Delta x)X_1(z) - Y(z) \tag{18}$$

Using the same technique, the Z-transform of the other interior grid fields, $X_3(z)$, $X_4(z)$,…, $X_N(z)$ can also be expressed as a combination of $X_1(z)$ and $Y(z)$.

$$\begin{aligned} X_3(z) &= [1 + 2\cos(2k_x\Delta x)]X_1(z) - 2\cos(k_x\Delta x)Y(z) \\ X_4(z) &= 4\cos(k_x\Delta x)\cos(2k_x\Delta x)X_1(z) - [1 + 2\cos(2k_x\Delta x)]Y(z) \\ &\ldots \end{aligned} \tag{19}$$

To construct the transfer function of the system, we consider a mesh-truncation boundary parallel to the y-axis and located at $x=a$. When implemented in an FDTD scheme, any linear, constant coefficient ABC enforced at $x=a$ can be expressed as a weighted polynomial of space- and time-shift operators as:

$$\begin{aligned} BU &= \left(-I + \sum_{i=-I}^{I}\sum_{j=-J}^{J}\sum_{k=1}^{K}\beta_{ijk}S_x^{-i}S_y^{-j}T^{-k} \right)U \\ &= -u_{m,l}^n + \sum_{i=-I}^{I}\sum_{j=-J}^{J}\sum_{k=1}^{K}\beta_{ijk}u_{m-j,l-k}^{n-i} = 0 \end{aligned} \tag{20}$$

Applying the Z-transform on (20), and using (12)-(19), we can obtain an equation relating the transfer function of the system expressed as

$$H(z) = \frac{Y(z)}{X_1(z)} \tag{21}$$

We assert that the FDTD simulation, along with an absorbing boundary condition is stable if and only if the Courant limit is satisfied, boundary scheme stability condition is satisfied, and *H(z)* has poles that are inside the unit disc.

Next, we apply the coupled stability analysis to Higdon's second- and third-order operators.

IV.3.2 Applications of Coupled Stability Analysis to Second-Order Higdon's ABC

Higdon's second-order Higdon's ABC is given by

$$B_2 U = \prod_{i=1}^{2} (I + a_i T^{-1} + b_i S^{-1} + c_i S^{-1} T^{-1}) U = 0 \tag{22}$$

Expressed in terms of the nodal fields, (22) becomes

$$\begin{aligned} u_m^n + 2a_i u_m^{n-1} + a_i^2 u_m^{n-2} + 2b_i u_{m-1}^n + (2a_i b_i + 2c_i) u_{m-1}^{n-1} \\ + 2a_i c_i u_{m-1}^{n-2} + b_i^2 u_{m-2}^n + 2b_i c_i u_{m-2}^{n-1} + c_i^2 u_{m-2}^{n-2} = 0 \end{aligned} \tag{23}$$

If α_i is constant, then, $a_i = a_1$, $b_i = b_1$, $c_i = c_1$, for $i=1, 2,3,\ldots$ Applying the Z-transform to (23), use the properties derived in (16)-(19), the system function of the second-order Higdon's ABC can be obtained

$$\begin{aligned} H(z) &= \frac{Y(z)}{X_1(z)} \\ &= -\frac{2b_1 + 2\cos(k_x \Delta x) b_1^2 + (2a_1 b_1 + 2c_1 + 4b_1 c_1 \cos(k_x \Delta x)) z^{-1} + (2a_1 c_1 + c_1^2 2\cos(k_x \Delta x)) z^{-2}}{(1 - b_1^2) + (2a_1 - 2b_1 c_1) z^{-1} + (a_1^2 - c_1^2) z^{-2}} \end{aligned} \tag{24}$$

The system of (24) is depicted in Fig. 33, where,

$$A_2 = -\frac{2b_1 + (2a_1 b_1 + 2c_1)z^{-1} + 2a_1 c_1 z^{-2}}{1 + 2a_1 z^{-1} + a_1^2 z^{-2}}, B_2 = -\frac{b_1^2 + 2b_1 c_1 z^{-1} + c_1^2 z^{-2}}{1 + 2a_1 z^{-1} + a_1^2 z^{-2}}.$$

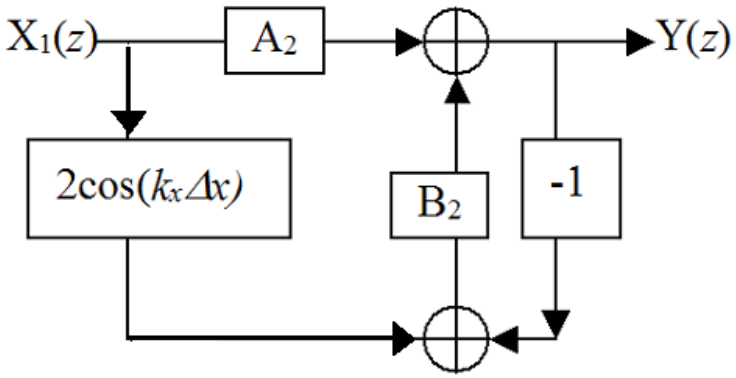

Fig. 33. Diagram of the system function of the second-order Higdon's ABC difference scheme

The poles of (24) are obtained by solving for the roots of the equation

$$(1 - b_1^2) + (2a_1 - 2b_1 c_1)z^{-1} + (a_1^2 - c_1^2)z^{-2} = 0 \qquad (25)$$

giving the two roots:

$$z_1 = -\frac{c_1 + a_1}{1 + b_1}$$
$$z_2 = -\frac{c_1 - a_1}{-1 + b_1}.$$

The norm of the two poles, with damping term $\alpha_i \Delta x = 0.0$, and $\alpha_i \Delta x = 0.0001$, are plotted in Fig. 34 (a) and (b), for the case $a=b$. The damping factor reduces the norm of the first pole to slightly less than unity as observed in Fig. 34 (b). Therefore, we conclude that for $a=b$, if and only if the damping factor term is nonzero, and $a=b \leq 0.5$, the second-order Higdon's ABC results in a stable FDTD scheme.

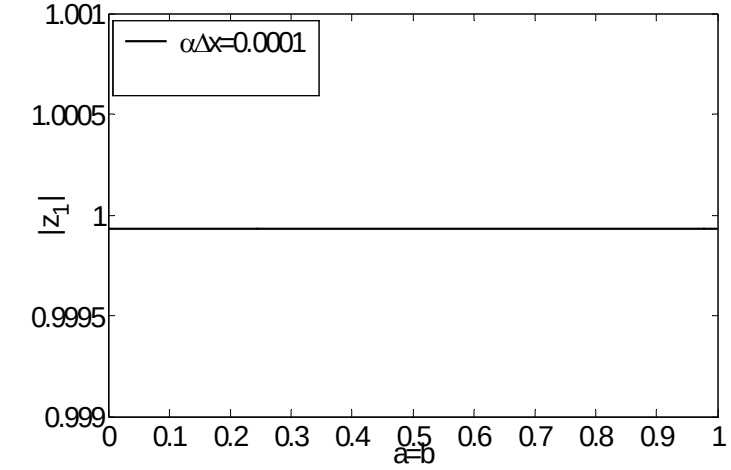

(a)

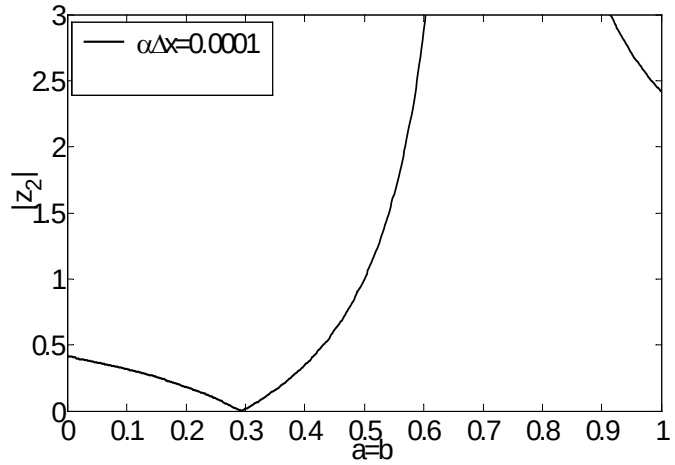

(b)

Fig. 34. The norms of the two poles for second-order Higdon's ABC (a) Norm of z_1; (b) Norm of z_2.

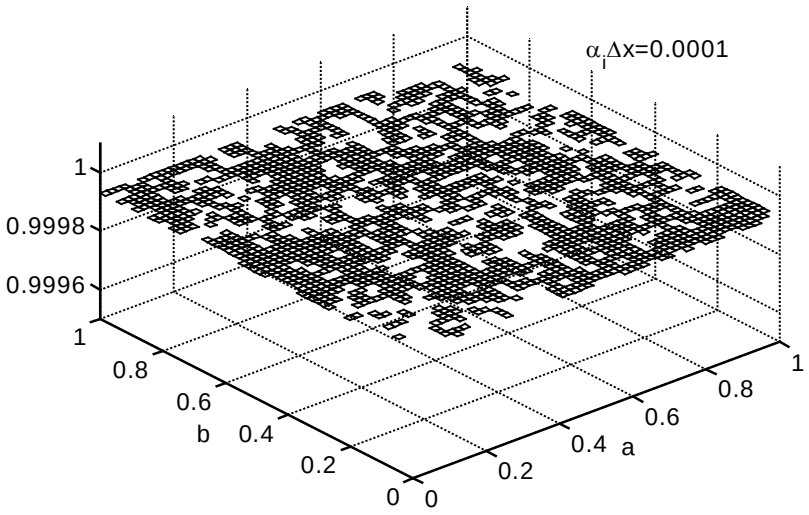

(a)

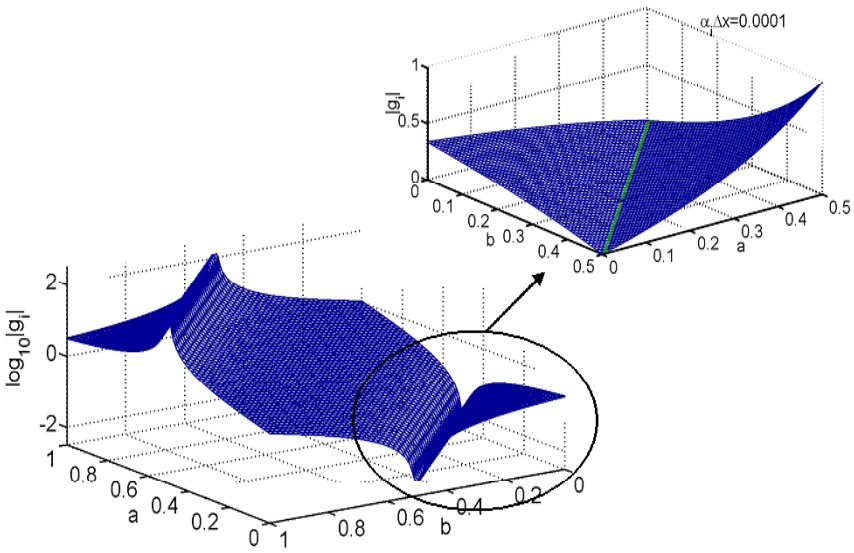

(b)

Fig. 35. The norms of poles for the second-order Higdon's ABC as a function of *a* and *b*, for $\alpha_i\Delta x$=0.0001 (a). Norm of z_1.; (b). Logarithmic plot of norm of z_2.

When $a \neq b$, the norms of the poles are plotted in Fig. 35 (a) and (b), in which the damping factor is set at $\alpha_i \Delta x = 0.0001$. Careful observation of the figures shows that the poles of the transfer function in (24) remain bounded for $a \leq 0.5$, $b \leq 0.5$, and $\alpha_i \Delta x > 0$. Therefore, we conclude that for the second-order Higdon ABC, a stable solution is obtained under the following conditions

$$\Delta t < \Delta t_c = \frac{1}{c\sqrt{\frac{1}{(\Delta x)^2} + \frac{1}{(\Delta y)^2}}}$$
$$0 < \alpha_i \Delta x \qquad (26)$$
$$a \leq 0.5, b \leq 0.5$$

Similar to the experiments discussed above, we consider a source placed at the center of a computational domain of size $40\Delta x$ x $40\Delta y$. The space step $\Delta x = \Delta y = 0.015$ m, and Δt subjected to the Courant limit. An observation point is chosen at $(+5\Delta x, +5\Delta y)$ with respect to the source. The field calculated at the observation point is shown in Fig. 36, for the case $a = b$. When the stability criterion (26) for the second-order Higdon's ABC is satisfied, the simulation result is stable. However, when (26) is not satisfied, the output becomes highly unstable as is clearly evident from Fig. 36. Fig. 37 shows the instability for case $a \neq b$, where the simulation results are fully consistent with the coupled stability analysis. For both cases, the damping term $\alpha_i \Delta x = 0.0001$.

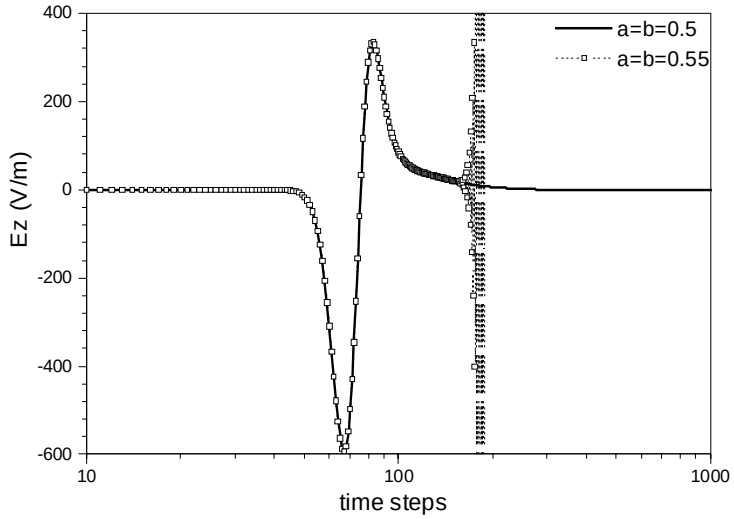

Fig. 36. Stability behavior of the second-order Higdon's ABC for case $a=b$.

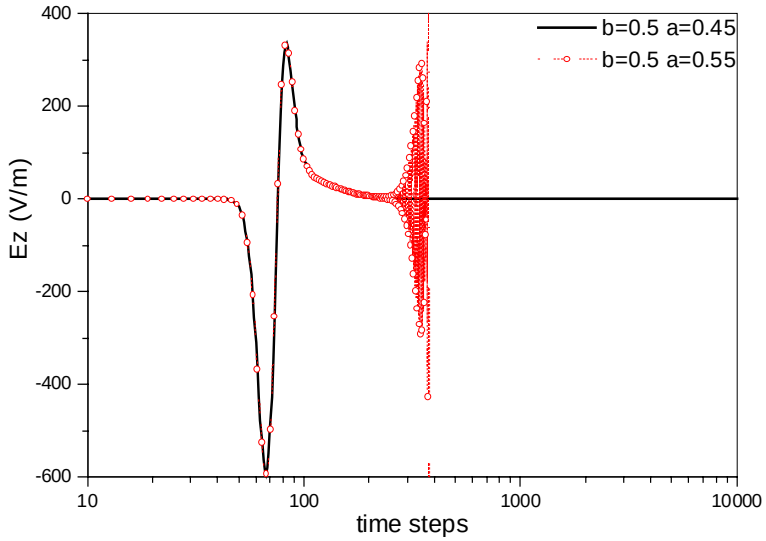

Fig. 37. Stability behavior of the second-order Higdon's ABC for case $a \neq b$.

IV.3.3 Applications of Coupled Stability Analysis to Third-Order Higdon's ABC

Similar to the analysis above, and applying the coupled stability analysis on Higdon third-order ABC, the system function defined by equation (21) is

$$H(z)=\frac{A_3+2B_3\cos(k_x\Delta x)+C_3e^{-jk_x\Delta x}}{1+B_3+2C_3\cos(k_x\Delta x)} \tag{27}$$

The system function is illustrated in Fig.14, in which

$$A_3=-\frac{-3b_1+(6a_1b_1-3c_1)z^{-1}+(6a_1c_1-3a_1^2b_1)z^{-2}-3a_1^2c_1z^{-3}}{1-3a_1z^{-1}+3a_1^2z^{-2}+a_1^3z^{-3}},$$

$$B_3=-\frac{3b_1^2+(6b_1c_1-3a_1b_1^2)z^{-1}+(3c_1^2-6a_1b_1c_1)z^{-2}-3a_1c_1^2z^{-3}}{1-3a_1z^{-1}+3a_1^2z^{-2}+a_1^3z^{-3}},$$

$$C_3=-\frac{-b_1^3-3b_1^2c_1z^{-1}-3b_1c_1^2z^{-2}-c_1^3z^{-3}}{1-3a_1z^{-1}+3a_1^2z^{-2}+a_1^3z^{-3}}.$$

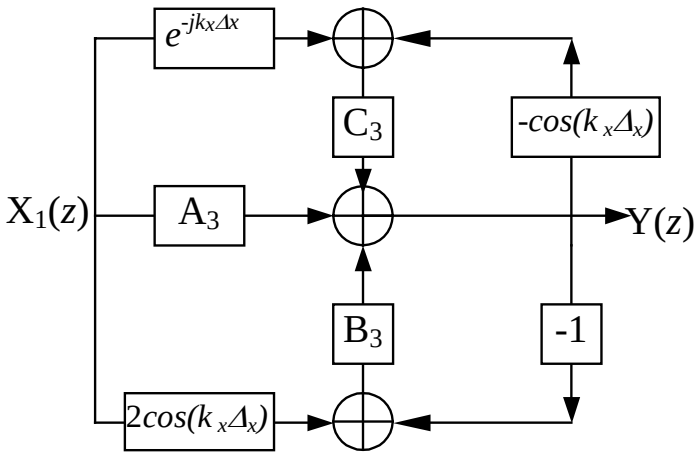

Fig. 38. Diagram of the system function of the third-order Higdon's ABC difference scheme.

Consequently, the poles are the roots of the following equation

$$(2\cos(k_x\Delta x)b_i^3 - 3b_i^2 + 1)z^3 + (6\cos(k_x\Delta x)b_i^2 c_i - 6b_i c_i + 3b_i^2 a_i - 3a_i)z^2 + (6\cos(k_x\Delta x)b_i c_i^2 + 3a_i^2 - 3c_i^2 + 6a_i b_i)z + (2\cos(k_x\Delta x)c_i^3 + 3a_i c_i^2 - a_i^3) = 0 \quad (28)$$

where, $k_x\Delta x \in [0, \frac{\pi}{2}]$, and, the $k_x\Delta x$ is dependent on the incident angle ϕ_i, for a specific wave and space stepping,

$$k_x\Delta x = k\cos\phi_i\,\Delta x = \frac{2\pi}{\lambda}\cos\phi_i\,\Delta x, \phi_i \in [0, \frac{\pi}{2}] \quad (29)$$

Equation (28) gives three poles, which are all dependent on the weighting functions *a*, *b* and the wave number k_x. For a stable scheme, the norms of the poles should be within the open-unit disc as $k_x\Delta x$ varies from 0 to $\pi/2$.

For the case $a=b$, the plots of the norms of the poles are shown in Fig. 39 (a), (b) and (c), for a damping factor of $\alpha_i\Delta x=0.0001$. (Again, we will not consider the case for $\alpha_i\Delta x=0.0$ as that violates the *boundary stability* criterion. It can easily be shown that coupled stability analysis also results in instability for $\alpha_i\Delta x=0.0$). Careful observation of Fig. 39 (a), (b) and (c), reveal that all three poles cannot be simultaneously less than unity, and consequently, stability cannot be guaranteed. For the case $a\neq b$, it suffices to consider the norm of the poles at $k_x\Delta x=0$. From Fig. 40, these norms, cannot be simultaneously less than unity. Therefore, we conclude that Higdon's third-order ABC results in an unconditionally instable FDTD scheme. *The instability cannot be eliminated by the introduction of damping factors.*

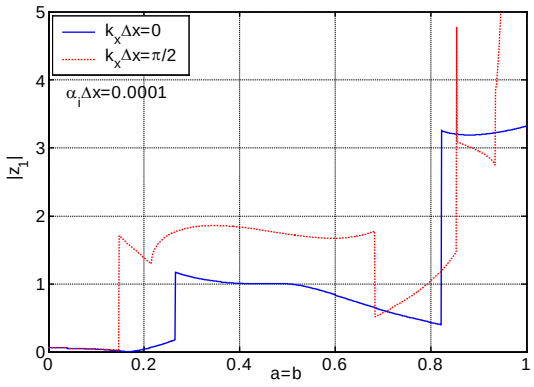

(a)

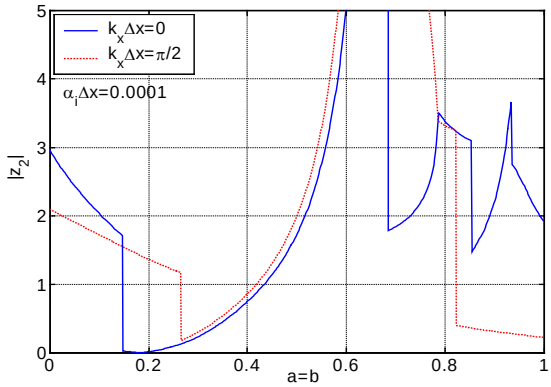

(b)

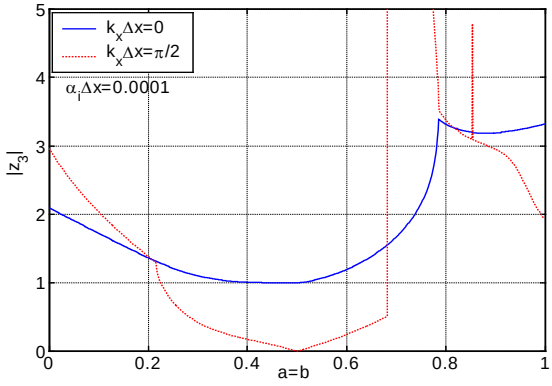

(c)

Fig. 39. Norms of poles of third-order Higdon ABC for *a=b and* for different incident angle $k_x\Delta x$.(a). Norm of z_1 (b). Norm of z_2; (c) Norm of z_3.

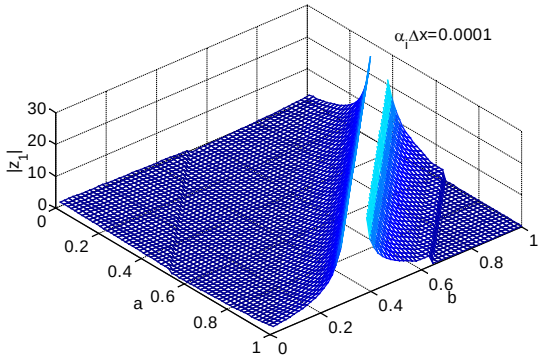

(a)

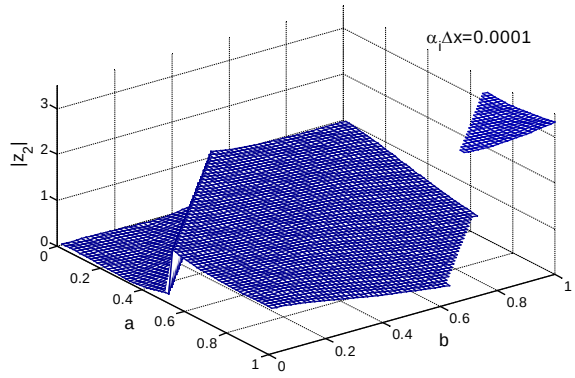

(b)

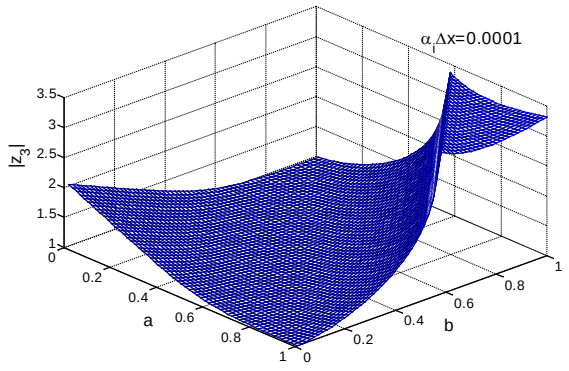

(c)

Fig. 40. Norm of poles of the third-order Higdon's ABC at $k_x\Delta x=0$ (a) Norm of z_1.; (b) Norm of z_2. (c) Norm of z_3.

As a numerical experiment, we consider the problem of a source radiating in a $40\Delta x$ x $40\Delta y$ two dimensional computational domain (with same source, observation point and space parameters as above). We show in Fig. 41 and Fig. 42 the effect of a and b on the stability behavior of the solution for the third-order Higdon ABC, while introducing a damping factor of $\alpha_i \Delta x = 0.0001$. Notice that the solution is always unstable irrespective of the choices for a and b, and, more importantly, the solution is unstable despite the non-zero positive damping factor.

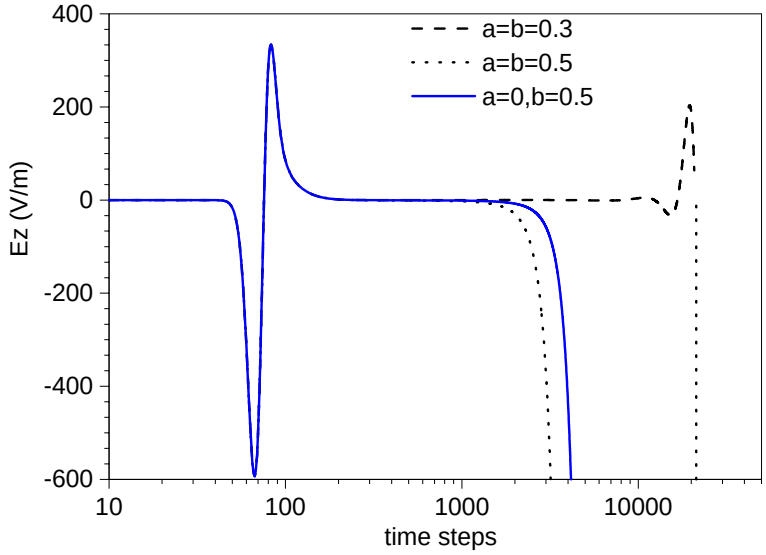

Fig. 41. Instability of the 3rd order Higdon's ABC for cases $a=b$ and $a \neq b$.

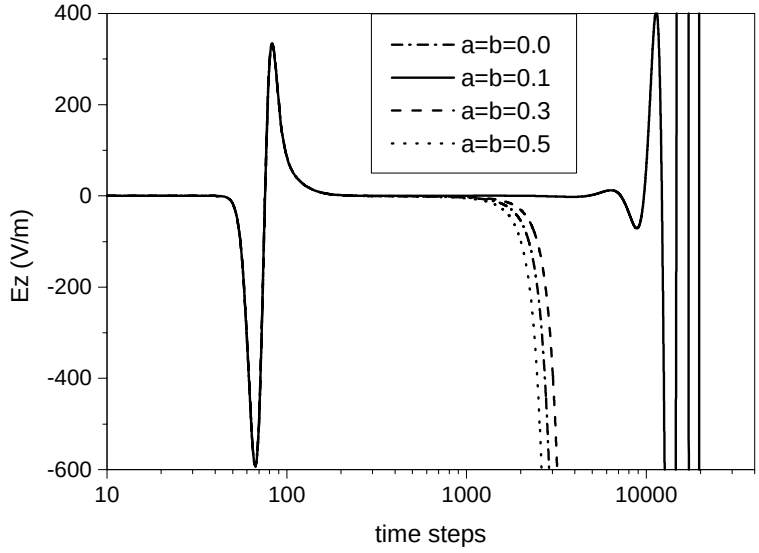

Fig. 42. Instability of the 3rd order Higdon's ABC when using series weighting functions *a=b*.

IV.4 CONCLUSIONS

In this chapter, a novel coupled stability analysis (CSA) method is developed to analyze the stability problems arising in the open-region FDTD simulations. The coupled stability analysis predicts that the second-order Higdon's ABC can be conditionally stable while the third-order Higdon's ABC is unconditionally instable. The numerical experiments in previous research work and presented here showed a good agreement with the predictions using CSA analysis.

V. WEIGHTED DIFFERENCE SCHEME AND DAMPING EFFECTS ON REFLECTION OF HIGDON'S ABC

When applying an ABC on boundary, the stability and absorption efficiency of the simulation are the most two important issues to be concerned. In the past, more attention has been paid on the absorption efficiency. However, stability issue is also critical: an instable boundary condition, or boundary difference scheme can result in an unstable simulation. The stability analysis when an ABC is applied to the truncated mesh is more complicated because it involves the interaction between the internal difference scheme and the boundary scheme.

The Higdon's ABC (HABC), which is a representative analytically derived ABC is important for its simplicity and high absorption (More discussion about Higdon's ABC can be found in section I.3.1). Based on the coupled stability analysis (CSA) method, which gives an efficient evaluation of the stability of the HABC, the stability of the criterion for the second order Higdon's ABC (HABC2), is given as following:

$$\begin{aligned} &\Delta t \le \frac{1}{c\sqrt{\frac{1}{(\Delta x)^2}+\frac{1}{(\Delta y)^2}}} \\ &0 < \alpha_i \Delta x < 1 \\ &a \le 0.5, b \le 0.5 \end{aligned} \quad , \qquad (1)$$

where Δt is the time increment; Δx, Δy are the space increment in x direction and y direction, respectively, and c is the speed of light. α_i is the damping factor, a and b are the weighting coefficients for difference formula.

For the third order or fourth order HABC, the FDTD simulation is unconditionally unstable.

Under the frame of stability requirements, the right choice of the weighting coefficients and damping factor becomes crucial for absorption efficiency. In this chapter, the absorption efficiency of weighted difference schemes and damping is investigated.

V.1 WEIGHTED DIFFERENCE SCHEME AND DAMPING EFFECTS ON REFLECTION OF HIGDON'S ABC

The magnitude of the reflection coefficient for the numerical finite difference formula of the second order Higdon's ABC is [7]:

$$|R| = \left| \prod_{i=1}^{2} \frac{1 - a_i e^{-j\omega\Delta_t} - b_i e^{jk_x\Delta_x} - c_i e^{jk_x\Delta_x} e^{-j\omega\Delta_t}}{1 - a_i e^{-j\omega\Delta_t} - b_i e^{-jk_x\Delta_x} - c_i e^{-jk_x\Delta_x} e^{-j\omega\Delta_t}} \right| \qquad (2)$$

where,

$$a_i = \frac{-(a - h(1-b))}{a - 1 - h(1-b) - \alpha_i \Delta x}$$

$$b_i = \frac{-(a - 1 + hb)}{a - 1 - h(1-b) - \alpha_i \Delta x}$$

$$c_i = \frac{-(-a - hb)}{a - 1 - h(1-b) - \alpha_i \Delta x}$$

$$h = \frac{\cos\phi_i}{C} \frac{\Delta x}{\Delta t}$$

for more details about parameters of Eq. (2), please refer to section IV.1.2.

Assume that the wavelength is $20\Delta x$, for different weighted schemes, the reflection minimized when $a=b=0.5$, as seen in Fig. 43. When a damping factor is applied to stabilize the boundary scheme, it will increase the reflection of the boundary

condition. For simplicity, we assume that the damping factor $\alpha_1 = \alpha_2 = \alpha$. Fig. 44 shows the relationship between reflection and damping factor term. It is seen that the relationship is non-linear: when damping factor term $\alpha\Delta x > 0.001$, the reflection increase dramatically against damping factor term $\alpha\Delta x$; when $\alpha\Delta x < 0.001$, the reflection is almost a constant (-220 dB).

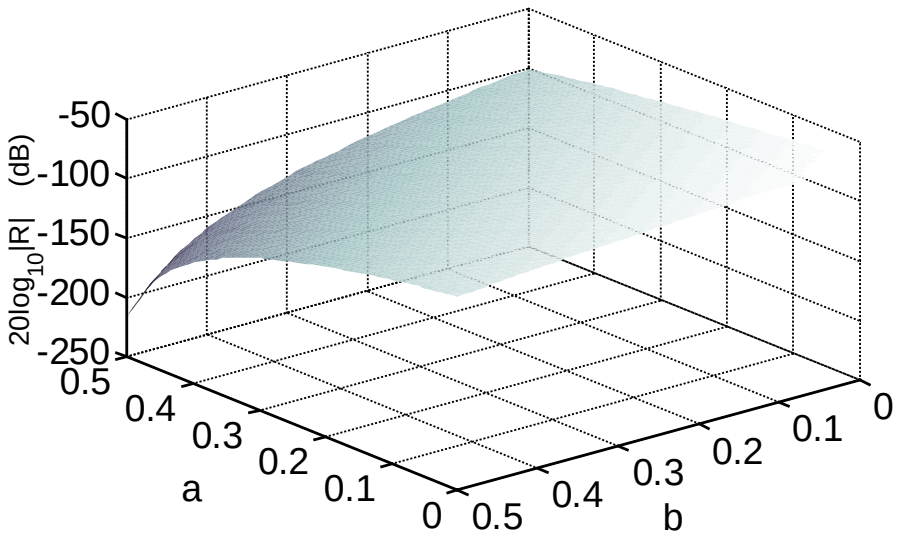

Fig. 43. Reflection of HABC2 when weighting functions a, b vary in [*0,0.5*].

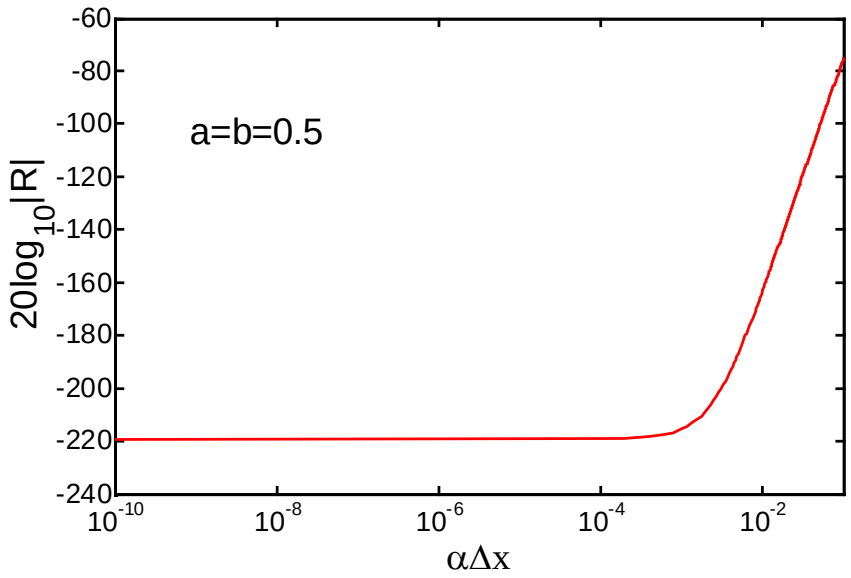

Fig. 44. Reflection vs. damping of the box difference scheme of Higdon's 2nd Order ABC.

The absorption efficiency is demonstrated by considering numerical experiments in 2-D space in which we study a problem that a Gaussian pulse is generated at the center and propagating in free space(TM polarization). The computational domain is 40×40 cells. For simplicity, we consider a uniform mesh in the x-direction and y-direction, with a space step $\Delta x=\Delta y=0.015$m and the time step $0.9\Delta t_c$, where Δt_c is the Courant limit. The temporal form is a Gaussian pulse. An observing point is set ($5\Delta x,5\Delta y$) offset from the source. The normalized error at the observing point, defined as

$$error = \log\left|\frac{E_{HABC2} - E_{ref}}{\max(E_{ref})}\right|$$

where E_{HABC2} is the solution obtained by using 2nd order HABC and E_{ref} is the numerical solution obtained devoid of observing any boundary reflections.

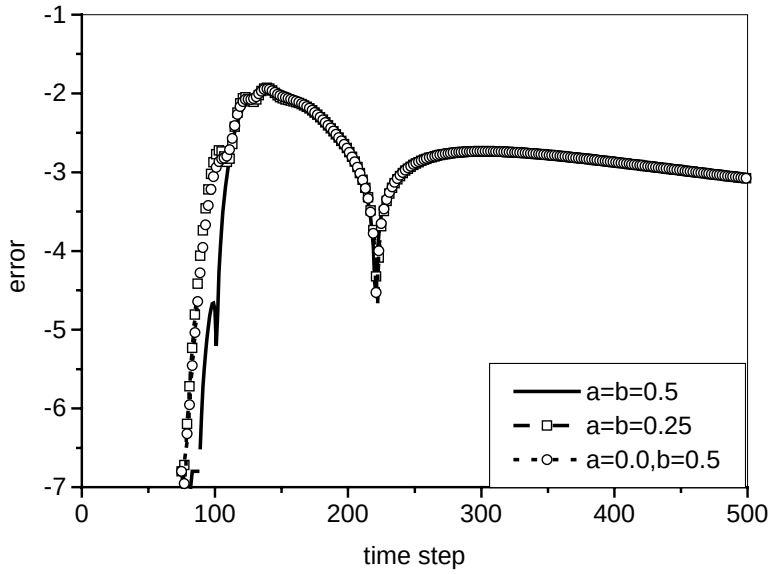

Fig. 45. Normalized simulation error of HABC2 obtained using weighted difference schemes with damping term $\alpha\Delta x=0.001$.

In the numerical experiments, three weighted difference schemes, the box scheme $a=b=0.5$, scheme 2($a=b=0.25$) and scheme 3 ($a=0.0, b=0.5$) with damping factor term $\alpha\Delta x =0.001$ and damping factor term $\alpha\Delta x =0.1$ are shown in Fig. 45 and Fig. 46. The box scheme with damping term $\alpha\Delta x =0.001$ gives the minimum errors, compared to the other combinations.

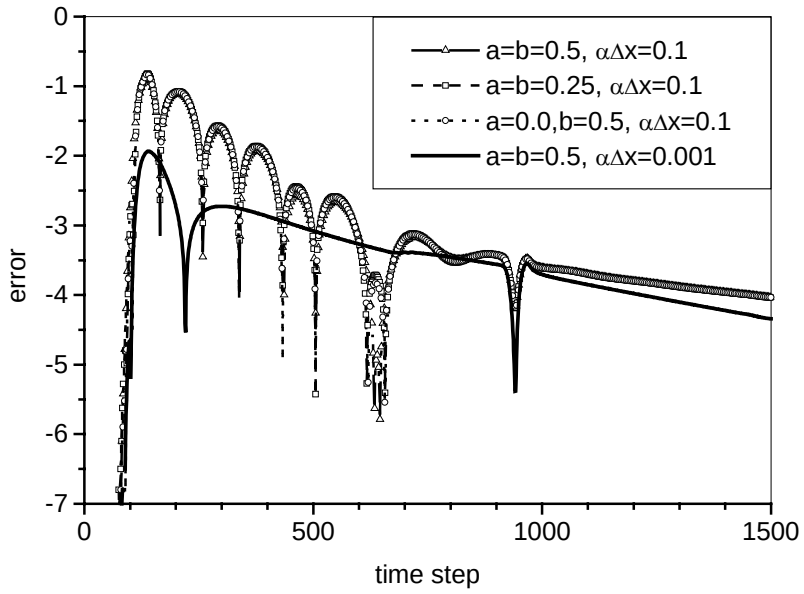

Fig. 46. Normalized error of HABC2 obtained using weighted difference schemes and damping factor term $\alpha\Delta x=0.1$, and the normalized error of the optimized difference scheme and damping factor.

V.2 CONCLUSIONS

Under the stability requirements, the weighting functions and damping factors are restricted when using finite difference approximation for the second-order Higdon's ABC. In this chapter, the optimized combination of weighting functions and damping are found to minimize the reflection. For the second-order Higdon's ABC, the box difference scheme and a damping constant less than $10^{-3}/\Delta x$ gives the minimum reflection.

APPENDIXES

A.1 FINITE VOLUME NUMERICAL TECHNIQUES IN ELECTROMAGNETICS

In this section, the finite volume numerical techniques used in this thesis are briefly described.

A.1.1 Yee Scheme and Finite Difference Time-Domain

In 1966, Kane Yee originated a set of finite-difference equations for the time-dependent Maxwell's curl equations system. The Yee scheme becomes the most useful finite-difference time-domain in computational electromagnetics since its fundamental basis is so robust. Namely:

A. Yee scheme solves for both electric and magnetic fields in time and space, using the coupled Maxwell's curl equations rather than solving for the electric field or the magnetic field alone with a wave equation.

B. As illustrated in , the Yee cell in the FDTD centers its **E** and **H** components in three dimensional space so that every **E** component is surrounding by four **H** components, and every **H** component is surrounding by four **E** components. This is extremely useful for specifying field boundary conditions and singularities. The finite-difference

expressions for the space derivatives used in the curl operators are central-difference scheme and of second-order accuracy.

C. The Yee scheme also centers its **E** and **H** components in time in what is termed a leapfrog arrangement. All of the **E** computations in the modeled space are completed and stored in memory for a particular time point using previously stored **H** data. Then all of the **H** computations in the space are completed and stored in memory using the **E** data just computed. It's a fully explicit and second-order accurate difference scheme.

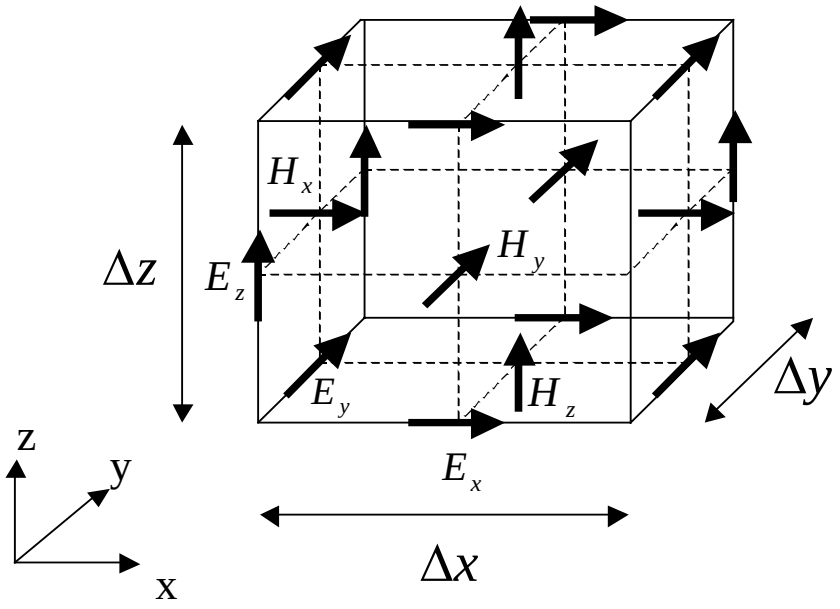

Fig. A. 1. The unit cell (Yee cell) used in Yee scheme.

The field in space is then denoted by the three indexes *i*, *j*, *k*, as

$$(i, j, k) = (i\Delta x, j\Delta y, k\Delta z) \tag{A.1}$$

then any field components *u* of **E** or **H**, can be written as

$$u(i\Delta x, j\Delta y, k\Delta z, n\Delta t) = u_{i,j,k}^{n} \tag{A.2}$$

The Yee cell in three-dimensional space is shown in Fig. A. 1 where the field components are staggered in space as before, such that they are a half-cell apart. Using the central difference scheme, Maxwell's equations transform to the following discrete finite-difference equations:

$$H_x^{n+\frac{1}{2}}(i,j,k) = H_x^{n-\frac{1}{2}}(i,j,k) + \frac{\Delta t}{\mu_{ijk}} \left[\begin{array}{l} \dfrac{E_y^n(i,j,k+1) - E_y^n(i,j,k)}{\Delta z} \\ -\dfrac{E_z^n(i,j+1,k) - E_z^n(i,j,k)}{\Delta y} \end{array} \right] \tag{A.3}$$

$$H_y^{n+\frac{1}{2}}(i,j,k) = H_y^{n-\frac{1}{2}}(i,j,k) + \frac{\Delta t}{\mu_{ijk}} \left[\begin{array}{l} \dfrac{E_z^n(i+1,j,k) - E_z^n(i,j,k)}{\Delta x} \\ -\dfrac{E_x^n(i,j,k+1) - E_x^n(i,j,k)}{\Delta z} \end{array} \right] \tag{A.4}$$

$$H_z^{n+\frac{1}{2}}(i,j,k) = H_z^{n-\frac{1}{2}}(i,j,k) + \frac{\Delta t}{\mu_{ijk}} \left[\begin{array}{l} \dfrac{E_x^n(i,j+1,k) - E_x^n(i,j,k)}{\Delta y} \\ -\dfrac{E_y^n(i+1,j,k) - E_y^n(i,j,k)}{\Delta x} \end{array} \right] \tag{A.5}$$

$$E_x^{n+1}(i,j,k) = E_x^n(i,j,k) + \frac{\Delta t}{\varepsilon_{ijk}} \left[\begin{array}{l} \dfrac{H_z^{n+\frac{1}{2}}(i,j+1,k) - H_z^{n+\frac{1}{2}}(i,j,k)}{\Delta y} \\ -\dfrac{H_y^{n+\frac{1}{2}}(i,j,k+1) - H_y^{n+\frac{1}{2}}(i,j,k)}{\Delta z} \end{array} \right] \tag{A.6}$$

$$E_y^{n+1}(i,j,k) = E_y^n(i,j,k) + \frac{\Delta t}{\varepsilon_{ijk}} \left[\begin{array}{l} \dfrac{H_x^{n+\frac{1}{2}}(i,j,k+1) - H_x^{n+\frac{1}{2}}(i,j,k)}{\Delta z} \\ -\dfrac{H_z^{n+\frac{1}{2}}(i+1,j,k) - H_z^{n+\frac{1}{2}}(i,j,k)}{\Delta x} \end{array} \right] \tag{A.7}$$

$$E_z^{n+1}(i,j,k) = E_z^n(i,j,k) + \frac{\Delta t}{\varepsilon_{ijk}} \left[\frac{H_y^{n+\frac{1}{2}}(i+1,j,k) - H_y^{n+\frac{1}{2}}(i,j,k)}{\Delta x} - \frac{H_x^{n+\frac{1}{2}}(i,j+1,k) - H_x^{n+\frac{1}{2}}(i,j,k)}{\Delta y} \right] \quad \text{(A.8)}$$

where ε_{ijk} and μ_{ijk} correspond to the permittivity and permeability of each cell in the mesh.

The order for calculating the fields is illustrated in Fig. A. 2. First, the electric field components are calculated; second, time is advanced one half-step; and third, the magnetic field is updated from the previously calculated electric field. This sequence is then repeated for all time steps.

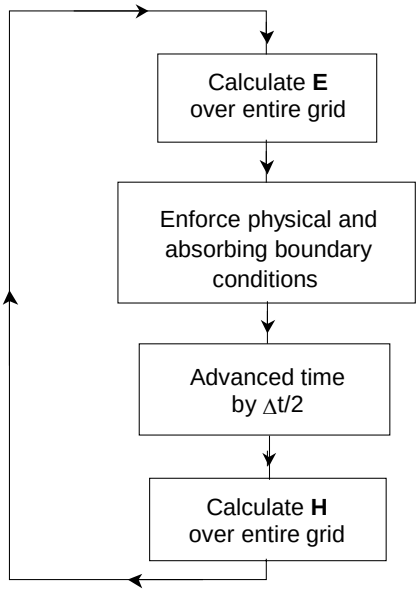

Fig. A. 2. Sequence of Field Calculation Within the FDTD Algorithm

A.1.2 Finite Difference Frequency Domain

The FDFD method in electromagnetics is to solve the time-harmonic Maxwell's equations in frequency domain. For a simple medium, the homogeneous Helmholtz's equations are subject to:

$$\nabla^2 u + k^2 u = 0 \tag{A.9}$$

where u can be any component of **E** or **H** in Cartesian coordinates system, and k is wave number in the medium. Therefore, for any component of **E** or **H**, using the central-difference scheme illustrated in Fig. A. 3, the finite difference frequency domain formulation of the two-dimensional, equal spaced ($\Delta=\Delta x=\Delta y$), homogeneous Helmholtz's equation is

$$\frac{u(i-1,j) + u(i+1,j) + u(i,j+1) + u(i,j-1) - 4u(i,j)}{\Delta^2} + k^2 u(i,j) = 0 \tag{A.10}$$

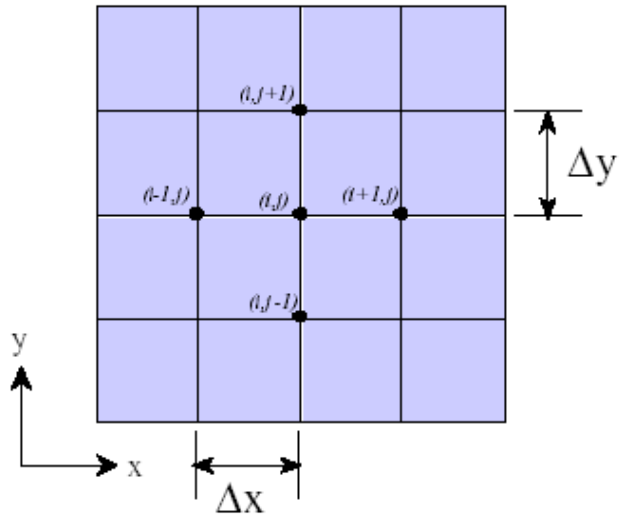

Fig. A. 3. The central-difference scheme.

A.1.3 Finite Element Method

The inhomogeneous Helmholz wave equation in two-dimensional space is given by:

$$[\nabla^2 + k(x,y)^2]u(x,y) = g(x,y) \qquad \text{(A.11)}$$

where $k(x,y)$ is the wave number in the medium, and g is a known excitation function.

The Helmholz equation describes the radiation of waves for TE-polarized or TM-polarized fields. Here, the use of the FEM is demonstrated in solving the Helmholz equation for the TM polarization where u represents the E_z. The remaining two field components, H_x and H_y, can be found from E_z, using Maxwell's equations.

The construction of a functional for (A.11):

$$F(u) = \int_{\Omega} (\nabla^2 u + k^2 u)u - 2gud\Omega \qquad \text{(A.12)}$$

This form can be simplified by invoking Green's theorem, which gives the following identity:

$$\int_{\Omega} (u\nabla^2 u + \nabla u \cdot \nabla u)d\Omega = \int_{\Gamma} u\frac{\partial u}{\partial n}d\Gamma \qquad \text{(A.13)}$$

Substituting (A.11) in (A.14), we have:

$$F(u) = \int_{\Omega} \nabla u \cdot \nabla u - k^2 u^2 - 2gud\Omega - \int_{\Gamma} u\frac{\partial y}{\partial n}d\Gamma \qquad \text{(A.14)}$$

Therefore, the variation of the functional

$$\delta F(u) = 0 \qquad \text{(A.15)}$$

gives the exact solution of the inhomogeneous Helmholtz equation.

In finite element methods, the unknowns, *u(x,y)*, are denoted as a function of nodal values, u_k,

$$u(x,y) = \sum_{k=1}^{M} N_k u_k, \qquad k = 1,2,3,... \tag{A.16}$$

where N_k is the shape functions. And the excitation, *g(x,y)*, is also denoted as a function of the nodal values, g_k, similar to the unknowns,

$$g(x,y) = \sum_{k=1}^{M} N_k g_k, \qquad k = 1,2,3,... \tag{A.17}$$

Substituting (A.16) and (A.17) into (A.15), we finally have a matrix system

$$\mathbf{M}\{u_k\} = \{g_k\} \tag{A.18}$$

where **M** denotes the coefficient matrix.

A.2 Z-TRANSFORM

In this section, the Z-transform and its important properties used in this thesis are briefly described.

The Z-transform of a given discrete signal, $x[n]$, is given by:

$$\mathcal{Z}[x[n]] = X(z) = \sum_{k=-\infty}^{\infty} x[n] z^{-n} \tag{A.19}$$

where z is a complex variable. The above definition is for a non-causal signal, i.e. $x[n]$ is known for time index, $n<0$. In most cases the signal will be causal giving rise to the One-Sided Z-transform:

$$\mathcal{Z}[x[n]] = X(z) = \sum_{k=0}^{\infty} x[n] z^{-n} \tag{A.20}$$

The Z-transform has many important properties. Here, we just discuss its linearity and shift property, which are critical for our coupled stability analysis.

Linearity:

Consider two sequences $x[n]$ and $y[n]$ with Z-transforms $X(z)$ and $Y(z)$, respectively, then

$$\mathcal{Z}[aX[n]+bY[n]]=aX[z]+bY[z] \tag{A.21}$$

where a and b are constants.

Shift of sequence:

Consider a sequence $x[n]$ such that Z-transform of the sequence is $X(z)$, then for the sequence whose values are $x[n+n_0]$, we have

$$\mathcal{Z}[X[n+n_0]]=z^{n_0}X[z] \tag{A.22}$$

REFERENCES

[1] G. D. Smith, *Numerical Solutions for Partial Differential Equations,* Oxford University Press, New York, 1985.

[2] K. W. Morton and D. F. Mayes, *Numerical Solutions for Partial Differential Equations: An Introduction*, Cambridge University Press, Cambridge, 1994.

[3] J. C. Strikwerda, *Finite Difference Schemes and Partial Differential Equations* , Wadsworth & Brooks/Cole Advanced Books & Software, Pacific Grove, CA, 1989.

[4] J. A. Kong, *Electromagnetic Wave Theory*, second edition, Johns Wiley and Sons, New York, 1990.

[5] M. N. O. Sadiku, *Numerical Techniques in Electromagnetics*, second edition, CRC Press LLC, New York, 2000.

[6] A. Taflove and S. C. Hagness, *Computational Electrodynamics: the Finite-Difference Time-Domain Method*, second edition, Artech House, New York, 2000.

[7] R. L. Higdon, "Absorbing boundary conditions for difference approximations to the multi-dimensional wave equation," *Math. Comp.*, vol. 47, no.176, pp.437-459, 1986.

[8] R. L. Higdon, "Absorbing boundary conditions for acoustic and elastic waves in stratified media," *J. Comp. Phys.*, vol. 101, pp. 386–418, 1992.

[9] B. Engquist and A. Majda, "Radiation boundary conditions for the numerical simulation of waves," *Math. Comput.* vol. 31, pp. 629-651, 1977.

[10] A. Bayliss and E. Turkel, “Radiation boundary conditions for wave-like equations,” *Commun. Pure Appl. Math.*, vol. 23, pp. 707–725, 1980.

[11] G. Mur, “Absorbing boundary conditions for the finite-difference approximation of the time-domain electromagnetic-field equations,” *IEEE Trans. Electromag. Comp.*, vol. 23, No. 4, pp. 377-382, Nov. 1981.

[12] E. L. Lindman, “Free-space boundary conditions for the time dependent wave equation,” *J. Comp. Phys.*, vol. 18, pp. 66-78, 1975.

[13] R. Mittra and O. M. Ramahi, “Absorbing boundary conditions for the direct solution of partial differential equations arising in electromagnetic scattering problems,” in *Finite Element and Finite Difference Methods in Electromagnetic Scattering*, M. Morgan, Ed., vol. 2, pp. 133-173, Elsevier Science, New York, 1989.

[14] R. L. Higdon, “Radiation boundary conditions for dispersive waves,” *SIAM J. Numer. Anal.*, vol. 31, No. 1, pp. 64-100, Feb. 1994.

[15] J.-P. Berenger, “A perfectly matched layer for the absorption of electromagnetic waves,” *J. Comput. Phys.*, vol. 114, pp. 185-200, 1994.

[16] O. M. Ramahi, “Complementary operators: A method to annihilate artificial reflections arising from the truncation of the computational domain in the solution of partial differential equations,” *IEEE Trans. Antennas Propagat.*, vol. 43, No. 7, pp. 697-704, July 1995.

[17] O. M. Ramahi, “The concurrent complementary operators method for FDTD mesh truncation,” *IEEE Trans. Antennas propagat.*, vol.46, No. 10, pp.1475-1482, Oct. 1998.

[18] O. M. Ramahi, “Concurrent complementary operators for mesh truncation in frequency-domain simulations,” *IEEE Microwave and Wireless Components Lett.,* vol. 12, No. 3, pp 99-101, March 2002.

[19] C. T. Law, and X. Zhang, “Concurrent complementary operator boundary conditions for optical beam propagation,” *IEEE Photonics Tech. Lett*., vol. 12, No. 1, pp. 56-58, Jan. 2000.

[20] C. W. Rowley and T. Colonius, “Discretely nonreflecting boundary conditions for linear hyperbolic systems,” *J. Comput. Phys.*, vol. 157, pp.500-538, 2000.

[21] Z. P. Liao, H. L. Wong, et al., “A transmitting boundary for transient wave analyses”, *Scientia Sinica (Series A)*, vol. 27, no. 10, pp. 1063-1076, 1984.

[22] M. Moghaddam and W. C. Chew, “Stabilizing Liao's absorbing boundary conditions using single precision arithmetic,” *IEEE Antennas and Propagat. Soc. Int. Symp.* London, Ontario, vol. 1, pp. 430-433, 1991.

[23] R. L. Wagner and W. C. Chew, “An analysis of Liao's absorbing boundary condition,” *Journal of Electromagnetic Waves and Applications*, vol. 9, pp.993-997, 1995.

[24] B. J. Zook, “A dispersive outer radiation boundary condition for FDTD calculations,” *10th Annual Review of Progress in Applied Computational Electromagnetics*, Monterey, California, vol.1, pp. 240-243, 1994.

[25] R. L. Higdon, “Radiation boundary conditions for elastic wave propagation,” *SIAM, J. Numer. Anal.* vol. 27, pp. 831-870, 1990.

[26] T. Wang and A. C. Tripp, “FDTD simulation of EM wave propagation in 3-D media,” *Geophysics*, vol. 61, pp. 110-120, 1996.

[27] O. M. Ramahi, “Stability of absorbing boundary conditions,” *IEEE Trans. Antennas Propagat.*, vol. 47, pp. 593-599, 1999.

[28] X. Wu and O. M. Ramahi, “Application of the concurrent complementary operators method to numerically-derived absorbing boundary conditions,” *Microwave Optical Tech. Lett.*, vol. 32, No. 4, pp. 272-275, Feb. 2002.

[29] O. M. Ramahi, “Frequency-domain complementary operators for finite elements simulation,” *IEEE Trans. Antennas Propagat.,* vol. 48, No. 4, pp. 629-631, April 2000.

[30] O. M. Ramahi, “The concurrent complementary operators method for FDTD mesh truncation,” *IEEE Trans. Antennas propagat.,* vol. 46, No. 10, pp.1475-1482, Oct. 1998.

[31] O. M. Ramahi, “Concurrent complementary operators for mesh truncation in frequency-domain simulations,” *IEEE Microwave and Wireless Components Lett.,* vol. 12, No. 3, pp 99-101, March 2002.

[32] O. M. Ramahi, “Exact implementation of higher order Bayliss-Turkel absorbing boundary operators in finite-elements simulation,” *IEEE Microwave Guided Wave Lett*., vol. 8, No. 11, pp. 360-362, Nov. 1998.

[33] A. C. Polycarpou, M. R. Lyons, and C. A. Balanis, “A two-dimensional Finite Element Formulation of the Perfectly Matched Layer”, *IEEE Microwave Guided Wave Lett.*, vol. 6, no. 11, pp. 338-341, Sept. 1996.

[34] R. F. Harrington, *Time-Harmonic Electromagnetic Fields*, IEEE Press: Willey-Interscience, New York, 2001.

[35] K. S. Yee, “Numerical solution of initial boundary value problems involving Maxwell’s equations in isotropic media,” *IEEE Trans. Antenna and Propagation*, vol. 14, pp. 302-307, 1966.

[36] O. M. Ramahi and X. Wu, “Complementary operators and associated issues of instability,” *Proc. International Conference on Electromagnetics in Advanced Applications, ICEAA 2001*, Torino, Italy, pp. 373, 2001.

[37] J. Schneider, private communications, 2002.

[38] H.-O. Kreiss, “Initial boundary value problems for hyperbolic systems,” *Comm. Pure Appl. Math*., vol. 23, pp. 277-298, 1970.

[39] B. Gustafsson, H.-O. Kreiss, and A. Sundström, “Stability theory of difference approximations for initial boundary value problems II,” *Math. Comp.*, vol. 26, pp. 649-686, 1972.

[40] L. N. Trefethen, *Finite Difference and Spectral Methods for Ordinary and Partial Differential Equations* (unpublished text, 1996, available at http://web.comlab.ox.ac.uk/oucl/work/nick.trefethen/pdetext.html).

[41] L. N. Trefethen, private communications, 2002.

[42] R. L. Higdon, “Numerical absorbing boundary conditions for the wave equation,” *Math. Comp.*, vol. 49, no. 179, pp. 65-90, 1987.

[43] J. Fang, “Investigation on the stability of absorbing boundary conditions for the time-domain finite-difference method,” *IEEE Antennas and Propagat. Soc. Int. Symp.*, Chicago, IL, vol. 1, pp. 548-551, 1992.

[44] B. Archambeault, O. M. Ramahi and C. Brench, *EMI/EMC Computational Modeling Handbook*, Second Edition, Kluwer Academic, Boston, MA, 2001.

[45] E. Kamen, *Introduction to Signals and Systems*, Macmillan Publishing Company, New York, 1987.

[46] A. V. Openenheim, R. W. Shafer and J. R. Buck, *Discrete-Time Signal Processing*, second edition, Upper Saddle River, NJ, Prentice Hall, 1999.